

Comparative study of machine learning and deep learning methods on ASD classification

Ramchandra Rimal, Mitchell Brannon, Yingxin Wang
and Xin Yang

*Department of Mathematical Sciences, Middle Tennessee State
University, 612 Old Main Cir KOM, Murfreesboro, 37132, TN,
USA.

*Corresponding author(s). E-mail(s):

ramchandra.rimal@mtsu.edu;

Contributing authors: mb2at@mtmail.mtsu.edu;

yw3n@mtmail.mtsu.edu; Xin.Yang@mtsu.edu;

Abstract

The autism dataset is studied to identify the differences between autistic and healthy groups. For this, the resting-state Functional Magnetic Resonance Imaging (rs-fMRI) data of the two groups are analyzed, and networks of connections between brain regions were created. Several classification frameworks are developed to distinguish the connectivity patterns between the groups. The best models for statistical inference and precision were compared, and the tradeoff between precision and model interpretability was analyzed. Finally, the classification accuracy measures were reported to justify the performance of our framework. Our best model can classify autistic and healthy patients on the multisite ABIDE I data with 71% accuracy.

Keywords: rs-fMRI, machine learning, deep learning, ASD

1 Introduction

Brain Imaging Analysis is one of the emerging fields in cognitive neuroscience. Imaging studies reveal insights about normal brain function and structure,

neural processing and neuroanatomic manifestations of psychiatric and neurological disorders, and neural processing alterations associated with treatment response [1]. This study performs the imaging methods to identify Autism Spectrum Disorder (ASD). ASD is a developmental disability that may cause difficulties in communicating and interacting with others and challenge their learning ability. Children with ASD tend to exhibit repetitive behavior or fixate on a particular interest. ASD is one of the fastest-growing developmental disorders that affect communication and behavior in the United States [2]. The advancements in medicine and technology have allowed physicians to assess, diagnose, and treat the complexities of ASD utilizing non-invasive techniques. Specifically, advancements in Brain Imaging Analysis have given physicians and researchers a more robust understanding of brain development. Studies conducted have shown, using Brain Imaging Analysis, that those with ASD have altered brain connectivity due to the nature of accelerated growth in the brain during development [3]. According to the Centers for Disease Control and Prevention (CDC) data, the occurrence of diagnosis has increased over the years as 1 in 54 children are diagnosed with ASD. Unfortunately, achieving an accurate diagnosis is not always easy because it is based on heterogeneous behavior rather than measuring biological markers. Furthermore, there is no cure for ASD, but the most widely accepted forms of effective treatments include behavioral interventions [3]. Emphasizing early, accurate diagnosis can contribute to successful, albeit varying levels of success, patient outcomes due to earlier treatment interventions.

A popular tool used in neuroimaging is Functional Magnetic Resonance Imaging (fMRI) which looks at the magnetic properties given by fluctuating levels of oxyhemoglobin and deoxyhemoglobin, which are affected by fluctuating levels of neural activity. Thus, the fMRI detects this Blood Oxygen Level Dependent (BOLD) signal to create a 3D image of the brain. This has given physicians and researchers a deeper understanding of how brain activity works, and the implications on ASD are significant. fMRI is very popular because it is a non-invasive method to obtain neural activity information from the human brain. Currently, two modalities of the fMRI have been used, the rs-fMRI and task-based fMRI. In this article, we work with the rs-fMRI data. The rs-fMRI is a neuroimaging tool that measures spontaneous low-frequency fluctuations in the neural BOLD signal of a subject at rest to investigate the functional architecture of the brain [4]. Functional Connectivity (FC), a pairwise relationship between two brain regions, is considered an essential step in searching for neuro markers in the ASD subject. The functional organization of networks involved in social and emotional processing is different between autism and healthy individuals; thus, rs-fMRI can be used as a diagnostic tool for ASD [5]. Several supervised and unsupervised learning methods have been used in analyzing the rs-fMRI data based on FC. Unsupervised machine learning is suitable for analyzing high-dimensional data with complex structures [4]. Meanwhile, several supervised learning methods have been demonstrated

to assess the mapping between input features and corresponding target predictions. Since systematic alterations in resting-state patterns are reported to be associated with pathology or cognitive traits, analyzing rs-fMRI data using supervised methods could facilitate the accuracy of ASD diagnostics [6]. Khan et al. (2020) [7] implemented the sequential forward feature selection approach to obtain highly distinguishing features between autistic and healthy controls. The results in [8] show a decreased FC among the ASD subjects as compared to the controlled subjects. In the task unrelated neuronal activity between 23 ASD and 20 control subjects, the study in [9] found the disruptions in FC. The work on [10] focused on the model interpretability. They implemented linear classification techniques to classify not only ASD but also Alzheimer's and Schizophrenia. [11] implemented several classification techniques to classify ASD and normal patients and concluded that the neural networks outperformed other methods.

While the existing diagnostic methods for ASD have high accuracy for homogeneous and small data sets, the classification capacity is not sufficient for heterogeneous and multisite data [12]. Due to the complex nature of ASD and the difficulties presented in diagnosis, we seek to develop a more effective classification framework to improve the accuracy of ASD classification for heterogeneous and multisite data. Furthermore, we work on the classification of ASD based on FC, emphasizing the comparative study for interpretability of the model and the accuracy of the results.

2 Literature Review

Current machine learning diagnostic frameworks face challenges due to the heterogeneous nature of ASD data. This data derives information from fMRI and diffusion MRI, which may not directly capture relational, morphological changes between brain regions. Therefore, [13] performed crowdsourcing to create a pool of machine learning pipelines for the diagnosis of ASD using cortical morphological networks (T1-weighted MRI) in Kaggle competition. All methods laying the foundation of those pipelines were examined under three machine learning steps: preprocessing techniques, dimensionality reduction methods, and learning models. A total of 20 teams participated in the study, and their performances were ranked after evaluating the accuracy, sensitivity, and specificity metrics of their models. The first-ranked team achieved an accuracy of 0.7, the sensitivity of 0.725, and the specificity of 0.675, respectively, demonstrating its discriminative potential in diagnosing ASD. Wang et al. [6] implemented a support vector machine recursive feature elimination (SVM-RFE) method, a FC-based algorithm, to distinguish ASD from the control group. This study involved 255 ASD patients and 276 TD controls from 10 settings. Based on the social motivation hypothesis, 35 regions of interest were selected to construct the FC matrix. First, SVM-RFE was conducted to screen bioinformatics in the complex high-dimensional FC dataset using a stratified, 4-fold cross-validation approach. Then the selected

features were imported into the SVM with a Gaussian kernel for classification. The developed classification algorithm appeared to improve the classification accuracy for the overall test and the leave-one-site-out test. These results indicated the new classification algorithm's capacity to accurately measure the importance of features and select the subset of most discerning features, which was superior to the current similar studies.

In the paper, Dvornek et al. [12], the authors aimed to distinguish the ASD individuals from resting-state functional MRI time-series using long short-term memory (LSTM) networks. Utilizing the standardization of the time scale and data augmentation, 11000 input sequences from 1100 subjects consisting of 539 individuals with ASD and 573 typical controls from 17 international sites were analyzed in this study. The LSTM weights were applied to the data to account for both the current state and the signal from previous states; after stratified 10-fold cross-validation, the LSTM with 32 hidden nodes was found to achieve a classification accuracy of 68.5%. This model was demonstrated to provide high classification accuracy on large heterogeneous datasets, which opens the door for further studies to investigate the mechanism of ASD. Kong et al. [14] looked at standard classification methods used for ASD and sought to construct a deep neural network (DNN) classifier to diagnose ASD more efficiently. The researchers looked at small fMRI data consisting of 182 subjects, 78 of whom had ASD. They constructed an individual network for each subject utilizing the Destrieux atlas for parcellating different brain regions. Then the features that are extracted from the regions of interest (ROIs) are ranked using an F-score, which measures the discrimination of two sets of real numbers via the DNN classifier. Their classification method achieved about 90.39% accuracy, which was significantly higher when compared to other existing methods. The researchers repeated their experiment with another dataset, resulting in an 86.70% accuracy. Therefore, the researchers concluded that their proposed method was effective in ASD classification. It should be noted; however, the researchers looked at homogenous data sets juxtaposed to other research that utilized heterogeneous data sets. Heinsfeld et al. [15] wanted to accurately classify ASD patients, based on their brain activation patterns alone, by applying deep learning algorithms. The dataset used was rs-fMRI data from the Autism Imaging Data Exchange, which included 1,035 patients, 505 of whom were ASD patients. The study used two stacked denoising autoencoders to extract the information of the dataset. The results were compared to the Support Vector Machine (SVM) and the Random Forest (RF) models. The researchers of this study were able to achieve an accuracy of 70%, which was the highest classification achieved in comparison to the SVM and RF. The study concluded that deep learning methods might be a reliable way to classify ASD, despite data collected from different equipment and demographics. However, the study falls short of biomarker standards despite taking steps in the right direction towards more reliable results.

Anirudh et al. [16] proposed a new approach to generating sets of population graphs predictive modeling, which was a bootstrap version of graph convolutional neural network (G-CNNs). The authors used weakly trained G-CNNs and reduced the sensitivity of the model selection graph structure. The dataset used consists of 1112 patients of the Autism Brain Imaging Data Exchange (ABIDE) dataset. Results indicated that the accuracy of novel method prediction accuracy was 70.86%, which is superior to the G-CNNs's 69.50%. In the article, Thomas et al. [17] trained a full three-dimensional convolutional neural network (3D-CNN) on a cohort of about 2000 cases of Autism Brain Imaging Data Exchange (ABIDE)-I and II] data set. In this method, the authors achieved an accuracy of 66%, which was comparable to the single measure regional homogeneity. In addition, they further applied the SVM method on ABIDE, which achieved an accuracy of 60%, suggesting that 3D-CNNs could not detect additional information from these temporal transformations that were more useful to recognize ASD from controls. The paper by Gazzar et al. [18] introduced the graph convolution networks (GCN), which was a semi-supervised deep learning approach for using rs-fMRI to predict the diagnosis of ASD. The authors implemented a tenfold cross validation and across-sites cross validation scheme on the 1-D convolutional network. On the combined ABIDE I and II datasets, an accuracy of 0.68 and 0.65 were achieved, respectively.

The study by Sherkatghanad et al. [19] seeks to build an automated framework that can accurately identify and classify ASD patients and control subjects. The architecture that was proposed was a convolutional neural network (CNN); however, the researchers also considered other learning methods such as SVM, K-nearest neighbors (KNN), and RF. Their proposed CNN framework achieved a 70.22% accuracy score on the ABIDE I rs-fMRI dataset. In this article, Li et al. [20] examined biomarkers to identify characteristics of ASD and proposed a novel whole-brain fMRI-analysis scheme to discriminate ASD. C3D convolution architecture was developed to capture 3D spatial features [21]. Since fMRI was comprised of temporal and spatial information, the authors explored the temporal statistics with the sliding window method. They also studied the spatial features using a 2-channel convolutional 3D deep neural network (2CC3D). The proposed method generated an F-score of 0.89 ± 0.05 , a mean of F-score improved over 8.5% compared to traditional machine learning models. Subbaraju et al. [22] proposed a spatial feature-based detection method for feature identification of ASD by using rs-fMRI for accurate diagnosis of ASD. To examine the performance for ASD diagnosis, the authors conducted a detailed study using the large-scale ABIDE dataset, stratified by different gender and age groups. As a result, the SFM method could detect ASD in 78.6% for adolescent males, 85.4% for adult males, 86.7% for adolescent females, and 95% for adult females, which was superior in comparison to other methods in the existing literature.

Wang et al. [23] proposed an ASD identification approach based on multi-atlas deep feature representation and ensemble learning. First, the authors calculated multiple FCs between each pair of regions based on different brain atlases from fMRI data of each subject and extracted these FCs as the original features. Then, to better classify ASD, they applied the stacked denoising autoencoder to perform the multi-atlas deep feature representation. Finally, they proposed a multilayer perceptron and an ensemble learning method to perform the final ASD identification task. The model was validated using a total of 949 patients (including 419 ASDs and 530 typical controls) from the ABIDE-I dataset. The authors achieved an accuracy of 74.52%, a sensitivity of 80.69%, specificity of 66.71%, and AUC of 0.8026, respectively, which demonstrated its discriminative potential in diagnosing ASD. Almuqhim et al. [24] devised a deep-learning model named ASD-SAENet for ASD classification using fMRI data. The sparse autoencoder (SAE) is an unsupervised machine learning method that results in the optimized extraction of features for classification. Subsequently, feeding extracted features into a deep neural network leads to a superior classification of fMRI brain scans that are more prone to ASD. ASD-SAENet model is trained to optimize the classifier while improving extracted features based on reconstructed data error and the classifier error. They evaluated the ASD-SAENet model to learn features from the large-scale ABIDE-I dataset. The results indicated that the ASD-SAENet model developed an accuracy of 70.8%, the sensitivity of 62.2 %, and specificity of 79.1% for the ABIDE-I dataset, which was superior to other methods in the existing literature. However, phenotypic features carry predictive information and are always available; they were less likely to be included in the model. To overcome this problem, six distinct classification approaches, including Phenotype-TS, RawPhenotype-LSTM, EncPhenotype-LSTM, RawPhenotype-rsfScore, EncPhenotype-rsfScore, and Phenotype-Target, were implemented by Dvornek et al. [25] to incorporate phenotypic data with rsfMRI into a single deep learning framework for classifying ASD. They tested the proposed architectures using a cross-validation framework on the cohort of ABIDE-I (including 527 ASDs and 571 typical controls). Among all developed models, the RawPhenotype-rsfScore, $D = 2$ method outperformed prior work by achieving a mean accuracy of 67.9% and a mean subject accuracy of 70.1%.

3 Methods

The rest of the paper is organized as follows. We start with providing a computational framework for this work in section 3.1. Then, a brief review of the LSTM and GRU neural networks with the pseudo-code for their implementation is provided in section 3.2. Then the data collection and preprocessing steps are discussed in section 3.3. Next, the methods for generating functional connectivity between the brain regions of interest are presented in section 3.4.

Next, the implementation of principal component analysis (PCA) for dimension reduction is described in section 3.5. The discussion on the experimental methods and the hyperparameter tuning procedure is discussed in section 4.1 and section 4.2, respectively. Next, the detailed results on the model performance are reported in section 4.3 respectively. In addition, the conclusion and discussion of results are presented in section 5. After the acknowledgment, the references used in this article are provided in the references section. Finally, the hyperparameter tuning results are provided in the appendix section, where section .1 and section .2 contains all the results for the hyperparameter tuning for LSTM and GRU methods on all RSFCs, respectively.

3.1 Computational Framework

The proposed model framework is presented via the schematic diagram in Figure 1. As outlined in the diagram, the proposed research starts with extracting the time series from the CC200 atlas proposed in [26]. Then the RSFCs were created using Pearson's correlation, Spearman's rank correlation, and the Partial correlation. The upper triangular elements of those connectivity matrices were extracted as the features. The dimension reduction technique, known as PCA, is implemented, and 871 subjects with 600 features were selected for the modeling. The classification models are constructed for all classification methods experimented, and the best value of hyperparameters is obtained. Next, using the best value of hyperparameters chosen, the final model is fit on the training data, and the model is applied to classify the ASD and healthy patients on the test data set. Finally, the performance of our model is evaluated using various measures such as accuracy, sensitivity, specificity, and AUC. The details of the procedures are provided in the corresponding sections and subsections.

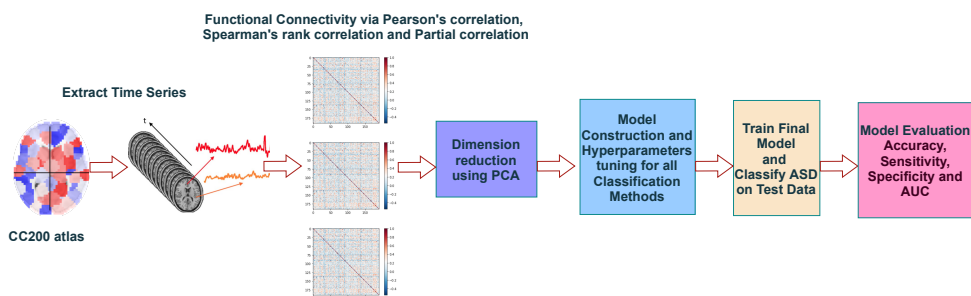


Fig. 1: Schematic diagram of proposed model framework

3.2 Review of Classification Techniques

This article experimented with several supervised learning methods such as Logistic Regression (LR), Linear Support Vector Classifier (LSVC), Kernel Support Vector Classifier (KSVC), Random Forest Classifier (RFC), AdaBoosting classifier (ABC), Gated Recurrent Unit (GRU), and LSTM neural networks. However, since LR, LSVC, KSVC, RFC, and ABC are standard classification techniques widely available in any popular statistics textbooks [27–29], an overview of these methods is not provided. So we provide the review of the neural networks based classification methods LSTM and GRU below.

A brief overview of LSTM

LSTM and GRU are popular and more recent variants of recurrent neural networks and have recently been used for ASD classification. We work on the ASD classification using the LSTM and GRU-based framework in this project. To understand LSTM and GRU models, first, we must understand the evolution of a Recurrent Neural Network (RNN) from a basic neural network. The structure of the basic neural network can be broken down into three components: input layer, hidden layer, and output layer. The Perceptron is the first trainable neural network and the simplest neural network with only one layer with adjustable weights and thresholds lying between input and output layers. RNN is a type of neural network that deals explicitly with time series or sequential data. RNNs are the improvements of the Feed-Forward Neural Networks (FFNN), where the signals can travel only one way from input to output. FFNNs can only read the current input layer and lacks an internal memory; therefore, these are bad at predicting what is to come. The most widely studied and used feed-forward neural network model is the multilayer FFNN, also called multilayer perceptrons. RNNs are called recurrent because they perform the same task for every element of a sequence, with the output being dependent on the previous computations. RNN is better than FFNN in modeling sequential data because RNN has a memory that captures the information about what has been calculated so far, and the output from the previous steps is taken as an input for the current stage. Hence, RNN makes a prediction, or a decision, based on its current input and the outputs from the previous step.

Mathematically speaking, the basic version of RNN has the form $h_t = g(Wx_t + W_h h_{t-1} + b)$, where x_t is the k dimensional input vector at time t , h_t the d -dimensional hidden state, g is the activation function (such as the logistic function, the hyperbolic tangent function, or the rectified Linear Unit), and $W \in \mathbb{R}^{d \times k}$, $W_h \in \mathbb{R}^{d \times d}$ are weight matrices, and $b \in \mathbb{R}^{d \times 1}$ is a bias vector [30]. As we can see, RNN is revolutionary compared to FFNNs, but there are some limitations. In the normal RNN cell, the input at a time step and the hidden state from the previous time step is passed through the

activation function to obtain a new hidden state and output where the gradients carry information used in the RNN parameter update. The parameter updates become insignificant when the gradient tends to zero, which means no real learning is done. On the other hand, when the error gradients accumulate during an update, the explosion occurs through exponential growth by repeatedly multiplying gradients through the network layers with values larger than 1, resulting in large gradients. These, in turn, result in large updates to the network weights and an unstable network. Hence due to the vanishing or exploding nature of the (stochastic) gradients with long sequences, RNN has difficulty in learning long-term dependencies [31–33]. For this reason, a different and improved architecture of RNNs was created called, LSTM.

LSTM essentially extends the memory of RNNs so that it can handle longer sequences of information. Unlike a standard RNN, which is comprised of the input, hidden, and output layers, LSTM has a memory cell that consists of an input gate, forget gate, and an output gate [34–37]. The most crucial component of LSTM architecture is the cell state which runs through the chain, with only linear interaction and keeping the flow of information unchanged. The gate mechanism of LSTM deletes or modifies the information of the cell state. First, the input gate decides which information is received, and then it goes through the forget gate, which determines if it is essential information to keep, and then it makes its way to the output gate. The LSTM utilizes a sigmoid function, a tanh function, and a pointwise multiplication operation to decide which information is passed through based on its importance. The architecture of LSTM at time t is presented in the Fig 2. In this figure, the four gates —output, change, input, and forget—are shown with their operations at time t . For a given input sequence $\{x_1, x_2, \dots, x_n\}$, $x_t \in \mathbb{R}^{k \times 1}$ is the input sequence at time t . The memory cell c_t updates the information using three gates: input gate i_t , forget gate f_t , and change gate \tilde{c}_t . The hidden state h_t is updated using output gate o_t and the memory cell c_t . The respective gates and layers compute the following functions at time t :

$$\begin{aligned} i_t &= \sigma(W_i x_t + W_{hi} h_{t-1} + b_i), \\ f_t &= \sigma(W_f x_t + W_{hf} h_{t-1} + b_f), \\ o_t &= \sigma(W_o x_t + W_{ho} h_{t-1} + b_o), \\ \tilde{c}_t &= \tanh(W_c x_t + W_{hc} h_{t-1} + b_c), \\ c_t &= f_t \odot c_{t-1} + i_t \odot \tilde{c}_t, \\ h_t &= o_t \odot \tanh(c_t) \end{aligned}$$

where, σ represent the sigmoid function. The operator \odot is the element-wise product, $W \in \mathbb{R}^{d \times k}$, $W_h \in \mathbb{R}^{d \times d}$ are weight matrices, and $b \in \mathbb{R}^{d \times 1}$ are bias vectors. Furthermore, n, k, d denotes the sequence length, the number of features, and the hidden size respectively [12, 39–41]. Several works on the literature during most recent years can be found on the fMRI data classification

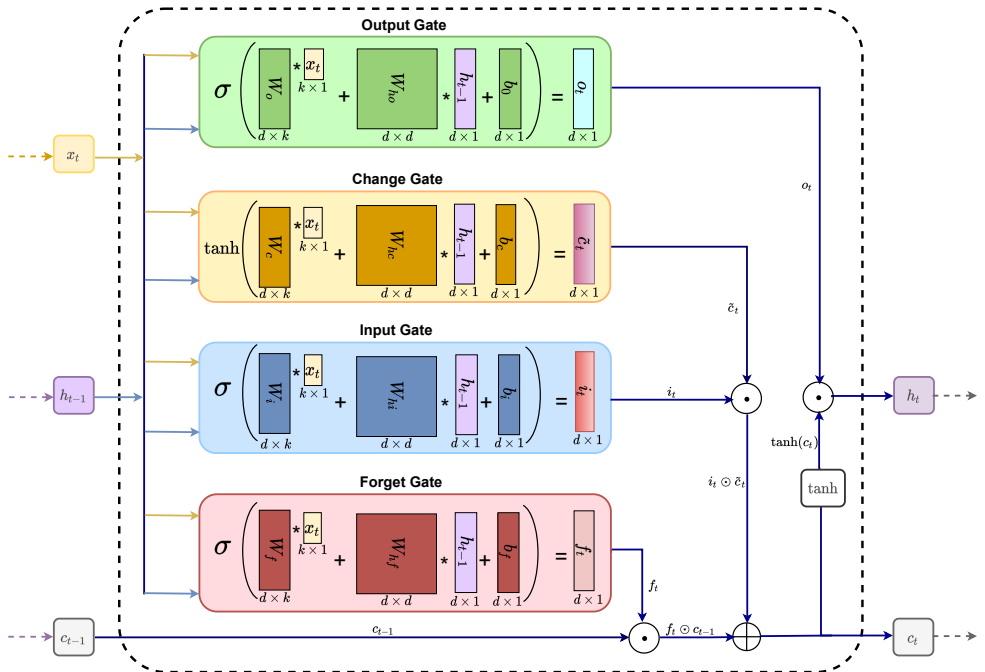


Fig. 2: Long short-term memory(LSTM) architecture [38].

using LSTM neural network [42–45]. In addition, to incorporate the required dimension of LSTM architecture, the input sequence X_t is created by taking m continuous sequence $x_t : x_{t+m-1}$ which is a matrix of shape $k \times m$ for $t \in \{1, 2, \dots, n - m - 1\}$. The output h_t of LSTM is a feature representation for the input sequence X_t at time t . Mathematically, h_t can be expressed as follows:

$$h_t = LSTM(X_t, h_{t-1}, c_{t-1}, w)$$

where w denotes all learnable parameters. Since the final hidden state h_f encodes the most information from the input sequence, it is converted to a vector using a dense layer.

A brief overview of GRU

GRU proposed by [46], is a relatively recent model inspired by LSTM that can deal with the vanishing or exploding nature of the (stochastic) gradients with long sequences. GRU minimizes or simplifies the three gates from the previous LSTM down to two. The two gates in GRU are called update and reset gates. The update gate is a combination of LSTM's input gate and the forget gate. Both the update gate and reset gate are two vectors that are calculated to determine which information goes through [47, 48]. The reset gate, denoted by r_t , is calculated by plugging in x_t and then multiplying by its weight W_r and then added with the multiplication of the previous information denoted

by h_{t-1} to its weights W_{hr} . These so-called weighted values, W_r and W_{hr} , are matrices. Next, the sigmoid function denoted by σ , is applied to the sum of the previous results, which will result in a real number that falls between 0 and 1. The reset gate decides how much information from the previous times should not go through. Then a tanh activation function, a nonlinear function which is denoted by \tilde{c}_t , is applied to assist in determining which information should be kept. Next, the update gate, denoted by u_t , is calculated similarly to the reset gate. However, the differences are in the weight matrices and the application of the update gate, which decides how much past information should go through. Finally, the final output is calculated by summing the element-wise multiplication to the update gate and the tanh function. The architecture of GRU at time t is presented in Fig 3. In this figure, the three gates —reset, change and update— are shown with their operations at time t . Similar as for LSTM model, for a given input sequence $\{x_1, x_2, \dots, x_n\}$, with

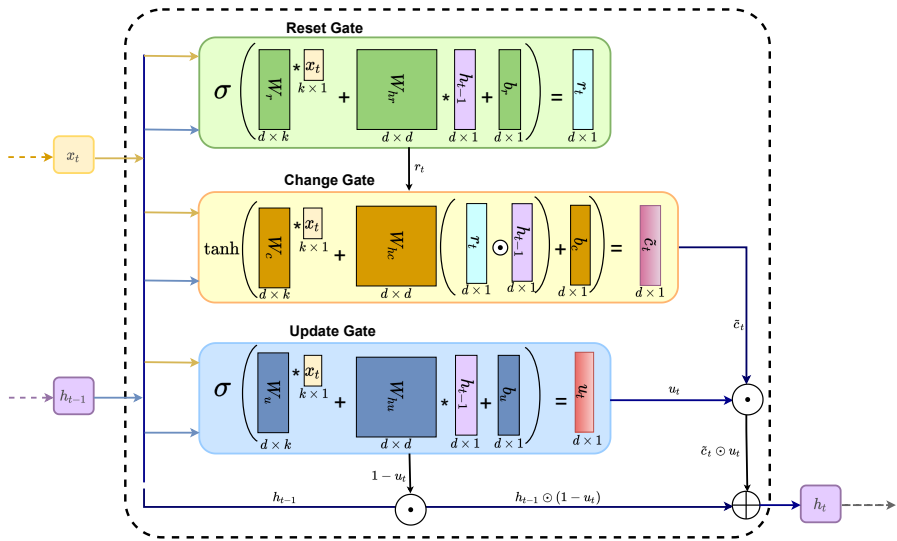


Fig. 3: GRU architecture [49].

$x_t \in \mathbb{R}^{k \times 1}$ the input sequence at time t . The gates and layers for the GRU model compute the following functions at time t :

$$\begin{aligned} r_t &= \sigma(W_r x_t + W_{hr} h_{t-1} + b_r), \\ u_t &= \sigma(W_u x_t + W_{hu} h_{t-1} + b_u), \\ \tilde{c}_t &= \tanh(W_c x_t + W_c (r_t \odot h_{t-1}) + b_c), \\ h_t &= (1 - u_t) \odot h_{t-1} + u_t \odot \tilde{c}_t \end{aligned}$$

where, σ represent the sigmoid function, \odot is the element-wise product; $W \in \mathbb{R}^{d \times k}$, $W_h \in \mathbb{R}^{d \times d}$ are weight matrices, and $b \in \mathbb{R}^{d \times 1}$ are bias vectors. In

addition, n, k, d denotes the sequence length, the number of features, and the hidden size respectively [47]. The input sequence X_t for the GRU model is created similarly as for the LSTM model. The output h_t of GRU is a feature representation for the input sequence X_t at time t , expressed mathematically as follows:

$$h_t = GRU(X_t, h_{t-1}, c_{t-1}, w)$$

where w denotes all parameters that can be learned by training the model.

Algorithms

The pseudo-code of our computational framework, especially the neural network-based GRU and LSTM models, is provided in this section. The algorithms for other machine learning models can be found in the [50]. Here, the algorithm 1 provides the pseudo-code for the hyperparameter tuning procedure for the LSTM and GRU models. Finally, the algorithm 2 shows how the LSTM and GRU models are incorporated in the computational framework for the ASD classification. The LSTM and GRU function were used from the keras-nightly 2.5.0. with the tensorflow version 2.5.0 for the computational work.

Algorithm 1 Pseudo Code for Hyperparameter Tuning Procedure for GRU/LSTM Model

Input Preparation: Read features after/without PCA transformation; Split train, validation and test data sets; and create input of the form [#subjects, time step, #features]

Model Input: [#subjects, time step, #features]; choices of optimizers, learning rates, and batch sizes.

Initialize: Set the number of epochs sufficiently large.

For “choice of optimizers”, **Do**

For “choice of learning rates”, **Do**

For “choice of batch sizes”, **Do**

For “range of number of replicates”, **Do**

Train the model, monitor validation loss;

Continue Until validation loss at epoch $n \leq$ validation loss at epoch $n + 1 \leq$ validation loss at epoch $n + 2$ Or maximum epochs reached.

Evaluate model on the validation data.

Calculate accuracy scores.

End Do.

Calculate average accuracy scores.

End Do.

End Do.

End Do.

Output Set of best hyperparameters, average accuracy scores, best average accuracy score.

Algorithm 2 Pseudo Code for GRU/LSTM Model

Input Preparation: Read features after/without PCA transformation; Split train and test data sets; and create input of the form [#subjects, time step, #features]

Model Input: [#subjects, time step, #features]; chosen hyperparameters (optimizer, learning rate, batch size) obtained from Algorithm 1 for each model.

Initialize: Set the number of epochs sufficiently large.

For “choice of neurons”, **Do**

For “range of number of replicates”, **Do**

 Train the model, monitor training loss;

Continue Until validation loss at epoch $n \leq$ validation loss at epoch $n + 1 \leq$ validation loss at epoch $n + 2$ Or maximum epochs reached.

 Evaluate model on the test data.

 Calculate accuracy, sensitivity, specificity and AUC scores.

End Do.

 Calculate minimum, maximum, average and standard deviation of accuracy, sensitivity, specificity and AUC scores.

 Save the results in respective files.

End Do.

3.3 Data Description and Preprocessing

ABIDE [51] initiative has aggregated functional brain imaging data collected from laboratories around the world to accelerate our understanding of the neural bases of autism. ABIDE is an open source for preprocessed neuroimaging data shared by the preprocessed connectomes project. We obtained the resting-state fMRI data from the ABIDE. Once rs-fMRI data are obtained, the first data analysis stage is preprocessing after initial quality control. The primary purpose of preprocessing is to reduce the effects of artifacts and other noise in preparation for FC analysis. The preprocessing of the ABIDE data was done with the X version of the Conjugate Analysis Scalable Pipeline (CPAC), which includes the following: slice time correction, motion correction, temporal filtering, skull stripping, nuisance regression, normalization, and registration. First, functional images were registered to anatomical space by a linear transformation, followed by white matter boundary-based transformation. The white matter boundary-based transformation was accomplished using FMRIB’s Linear Image Registration Tool of FMRIB Software Library and white matter tissue segmentation of FAST. The fMRI resting-state data is now ready for FC analysis after preprocessing. Many different functional atlases have been available such as CC200/CC400, BASC197/444, Power 264 region atlas, to name a few. ROIs generated from functional atlas, such as CC200/CC400, outperform the anatomical atlas (AAL, HO) in the context of resting-state FC analysis [26], [52]. Since we are focused on analyzing both interpretability and accuracy, the functional connectivity in this paper is calculated based on the functional atlas CC200. Figure 4 shows the brain ROIs of CC200 atlas. A total of 871

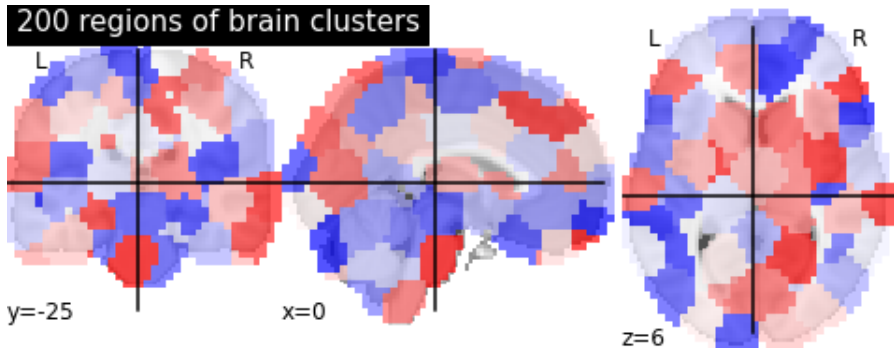


Fig. 4: CC200 atlas by Cameron and Craddock

subjects (observations) was selected for the analysis. The preprocessed fMRI data for each subject is a matrix of 196×200 where the matrix's first dimension(rows) represents the time points and the second dimension(columns) of the matrix depicts the brain regions of interest. The 200 brain regions of interest are obtained based on the functional atlas CC200. Among the 871 observations under consideration, 403 are autistic, and the remaining 468 are normal.

3.4 Generation of Functional Connectivity

After extracting the ROIs time series based on the CC200 atlas, the network of FC is created. We use three different methods to construct the connectivity matrix: Pearson's Correlation, Spearman's Rank Correlation, and Partial Correlation. The Pearson's correlation coefficient [53] is chosen as it is the widely used connectivity measure in the literature. On the other hand, partial correlation is claimed to be the better measure of the direct connectivity between the two brain regions stating that the correlation coefficient may seem to be higher; however, the correlation may be because of the influence of the other regions [[54], [55]]. In addition, Spearman's rank correlation [56] is used since it measures both linear and nonlinear relationships between the brain regions of interest. The connectivity matrices were symmetric ($m \times m$), where the upper diagonal elements were extracted into a feature vector of length $\frac{m(m-1)}{2}$. The elements on the diagonals were ignored as they represent the connections with themselves. Each feature represents the correlation between two regions of the brain conditioned on other regions. Here, we have data of the size $871 \times 19,900$ with the number of rows representing the number of subjects and the number of columns representing the features.

3.5 Dimension Reduction using Principal Component Analysis (PCA)

We have 871 observations with 19,900 features on each of them. Hence, we encounter the high-dimensional statistics-related problem where the number of features is much higher than the sample size. The PCA is implemented to mitigate the common challenges with high-dimensional data. For example, computational expense and an increased error rate due to multiple test corrections when testing each feature for association with an outcome. PCA simplifies the complexity in high-dimensional data by transforming the data into fewer dimensions which acts as summaries of features [57],[58]. After the PCA was implemented, around 80 percent of the data variability can be explained by 600 principal components. Figure 5 shows the percentage of variance explained by the principal components for all three different RSFC. The 600 principal

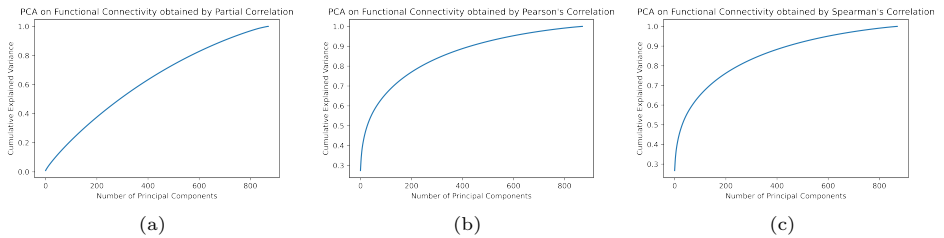


Fig. 5: The percentage of the variance explained by the number of principal components on the features obtained by (a)Partial Correlation, (b) Pearson's Correlation, and (c) Spearman's Correlation.

components that correspond to each type of FC were chosen. Each subject then has 600 features, each representing the principal components, and we have observations on the 871 subjects for the analysis. In this case, our data is of size 871×600 with the number of rows representing the number of subjects and the number of columns representing the number of principal components chosen. The experiment is performed on two types of data, one without PCA and another after applying PCA.

4 Experiments and Results

4.1 Experimental Methods

Several supervised learning methods such as LR, LSVC, KSVC, RFC, ABC, GRU, and LSTM neural networks are experimented in this article for ASD classification. The scikit-learn library [59], [60] and the TensorFlow [61] are mainly used for the implementation of the methods in python. The input for the models is the features vector obtained using three different methods for

constructing FC. The experiment is performed on two different types of data; features extracted from the original data with PCA and features extracted from the original data without PCA. First, ten-fold cross-validation is performed on the whole data to develop the classification model. Then, the best value of the parameters is selected from the model. Finally, the repeated ten-fold cross-validation is performed with these parameters, and the performance on the hold-out fold is reported. For stable performance, the experiment is replicated ten times. In addition, the feature selection method called the recursive feature selection technique was implemented. This technique takes all the features and drops the least important feature each time until the desired number of features to select is reached. In our analysis, the number of features is reduced to half of the total features whenever the recursive feature elimination method is implemented. The same procedure discussed above is repeated on the model with the application of recursive feature elimination and the model without implementing the recursive feature elimination method.

To fit the LSTM and GRU model, the necessary steps of the data preparation have been taken to prepare the input data as described below. The architecture for the LSTM neural network is presented in Figure 2. First, the input sequence is created using $k = 19,900$ features without dimension reduction ($k = 600$ after dimension reduction using PCA) with time step 1, as shown in the top part of the figure. Then at time $t - 1$, the input X_{t-1} , a matrix of size $k \times 1$, together with h_{t-2} and c_{t-2} is fed into the LSTM. For the next step, the output h_{t-1} of the previous step, together with input sequence X_t and the cell memory c_{t-1} become input for LSTM. This process continues until the final input sequence X_f with corresponding output h_f , a vector of length equal to the given number of neurons of the last LSTM layer. Finally, h_f is transmitted to a fully connected layer where the sigmoid function is used to predict the class of chess masters and chess novices. The transformed data at this point is a two-dimensional array (number of observations, number of features). However, the LSTM model expects three-dimensional input (number of observations, time step, number of predictors). Therefore, the time step of 1 is chosen to make the input data compatible with the model. Finally, the data is split randomly into two parts: 80% of the data is allocated for the training set, and the remaining 20% of the data is for the test set. The data preparation steps for GRU model is exactly same as of LSTM model.

For the LSTM and GRU models, the single-layer models have been implemented. For the models with various neurons ranges from 10 to 250, the hyperparameters to choose for each models are —the learning rate, the optimizers, the batch sizes, and the number of epochs. The various learning rates between 0.1 to 0.0001, the number of neurons between 10 to 250, the batch sizes in the range of 4 to 32, and the optimizers Adam, Adamax, and Nadam from Keras were experimented with. Once the best value of the hyperparameters is chosen, the model is fit on the training data using the hyperparameters

chosen, and the performance is evaluated on the test data set. Both LSTM and GRU models are also replicated ten times for stable model performance.

4.2 Hyperparameter Tuning

For the LR, L SVC, K SVC, ABC, and RFC models, the ten-fold cross-validation method was used to find the best value of the hyperparameters. LR was implemented with L_1 , L_2 , and elasticnet penalties. The feature selection techniques did not improve the results on the lasso penalty implemented version. The best result from the LR model was obtained using the feature selection method known as 'SelectFromModel' with a ridge penalty on logistic regression. For the K SVC model, the radial basis function kernel was used. For the RFC, the maximum depth of the tree between 5 and 20, the number of trees between 500 and 2500, and the node impurity criterion gini and entropy were compared, and the model with 2500 trees and the maximum depth of 5 were fitted using gini coefficient to minimize the node impurity. The AdaBoost classifier was implemented with a learning rate of 0.1, 0.01, and 0.001 and a number of trees between 500 and 1500. The model with a learning rate of 0.01 and 500 estimators was selected to build the final model.

For the LSTM and GRU model, the data set was divided into three parts, a training set, a validation set, and a test set. Initially, the data is split 80 percent into a training set and the remaining 20 percent into a test set. Then the 20% data from the training set is used for the validation set. The hyperparameters for the LSTM and GRU model are the batch sizes, the learning rate, the optimizers, and the number of epochs. We let the epochs be 100 and apply the early stopping criterion from the Keras library; the model will stop training if there is no improvement in the validation loss five consecutive times. Since the value of epochs is allowed to be sufficiently high, the early stopping criterion chooses the appropriate value of epochs. The remaining hyperparameters were chosen using hyperparameter tuning. The choice of the optimizers is Adam, Adagrad, and Nadam. The learning rate is chosen among the values of 0.01, 0.05, 0.001, 0.005, and 0.0001. The batch sizes of 4, 8, 16, and 32 were considered. The models with the number of neurons 10, 30, 50, 100, 150, 200, and 250 were compared. Overall, we have seven models for both LSTM and GRU neural networks. There are $5*4*3 = 60$ combinations for each of them, and the best combination among them is chosen using validation data. Since we have three sets of data obtained from Spearman RSFC, Pearson RSFCs, and Partial RSFCs, we performed the hyperparameter tuning for every data model. The best combination of hyperparameters was chosen that corresponds to the highest accuracy on the validation data. The chosen hyperparameters values were used to build the final model. For example, the hyperparameter tuning results for the 10 neurons single layer LSTM model is given in the Table 1. The best accuracy on the validation data was obtained with the batch size of 32 with a learning rate of 0.01 on the Adam optimizer, so these values of hyperparameters were chosen for the ten neurons single layer LSTM model. The hyperparameter tuning results for all other models are available in the

Table 1: Hyperparameter tuning for 10 neurons single layer LSTM on the Pearson's RSFC.

Optimizer	Learning rate	Batch size			
		4	8	16	32
Adam	0.01	0.6086	0.6136	0.6145	0.6163
	0.005	0.6126	0.6115	0.6116	0.6098
	0.001	0.6090	0.6102	0.6099	0.6094
	0.0005	0.6093	0.6093	0.6094	0.6091
	0.0001	0.6088	0.6091	0.6079	0.6063
Nadam	0.01	0.6070	0.6081	0.6081	0.6079
	0.005	0.6075	0.6077	0.6074	0.6068
	0.001	0.6052	0.6027	0.6004	0.5988
	0.0005	0.5971	0.5947	0.5924	0.5909
	0.0001	0.5890	0.5870	0.5847	0.5828
Adagrad	0.01	0.5838	0.5841	0.5844	0.5848
	0.005	0.5855	0.5859	0.5861	0.5867
	0.001	0.5874	0.5877	0.5878	0.5883
	0.0005	0.5887	0.5893	0.5895	0.5900
	0.0001	0.5903	0.5903	0.5903	0.5894

appendix from Table 1 - Table 41. Finally, the model fits the training data using the chosen hyperparameters, and the performance is evaluated on the test data set. For a stable model performance, each model is replicated ten times.

4.3 Model Performance

The developed framework is tested on classifying ASD patients with healthy patients. For the LR, SVC, KSVC, ABC, and RFC models, the selected value of parameters obtained from the grid-search cross-validation has been used in the repeated ten-fold cross-validation. The ten-fold cross-validation is replicated ten times, and the average accuracy, sensitivity, specificity, and AUC scores obtained from the hold-out fold are reported. In addition, the average performance scores from these methods implementing the recursive feature selection and the select from model techniques are recorded. The feature selection technique gives a mixed result with a smaller improvement in the accuracy of the LR model in comparison to without using model selection. The overall best performance is obtained from the logistic regression model with the feature selection. The best score was the accuracy of 71%, the sensitivity of 68%, specificity of 73%, and area under the curve score of 77%. The results

from the LSTM and GRU models are close to the best results obtained.

For the LSTM and GRU models, various single-layer models of 10, 30, 50, 100, 150, 200, and 250 neurons have been built with the best values of the hyperparameters chosen. The model is trained using the training data and tested on the 20% unseen data separated before the training. The early stopping criterion is implemented during the model training to stop training if there is no improvement in the loss for three consecutive times. We compare the results of the 21 models(seven models with three different RSFCs) for each of the LSTM and GRU. Each model is replicated ten times, and the average performance scores were reported for better reproducibility. Below, we report the best results for features obtained from each RSFC in a separate table. The following tables summarize the performance of all implemented methods obtained by using the Pearson's correlation, Partial correlation, and Spearman's rank correlation RSFC methods.

Table 2 summarizes the performance scores of the various supervised learn-

Table 2: Performance scores of the various supervised learning models on Partial RSFC using PCA

Metricses	Methods	KSVC	LSVC	LR +SFM	RFC	ABC	LSTM	GRU
	Min	47.13	43.68	43.18	47.12	51.15	58.86	59.43
Accuracy	Average	58.61	56.11	59.66	56.18	56.74	59.14	60.69
	Max	66.67	68.97	68.18	67.82	63.22	60.00	62.86
	Std	4.46	5.06	3.62	4.56	3.36	0.49	1.14
	Min	30	32.50	15.00	25	26.25	55.13	55.41
Sensitivity	Average	45.27	53.94	29.75	40.76	40.17	56.67	57.57
	Max	60.98	70	47.50	60	53.09	57.69	66.34
	Std	6.79	7.50	6.24	6.76	5.99	0.81	1.31
	Min	53.19	42.55	74.47	56.52	59.57	59.79	60.40
Specificity	Average	70.08	58	85.41	69.45	71	61.13	62.97
	Max	85.11	72.34	95.74	85.11	81.91	61.86	66.34
	Std	6.70	6.45	5.12	6.42	5.77	0.70	1.88
	Min	48.30	42.50	52.01	42.71	50.63	58.46	59.60
AUC	Average	61.52	56.69	64.36	57.55	57.45	58.78	60.61
	Max	74.02	71.49	78.47	71.85	66.36	59.25	61.37
	Std	5.22	5.42	5.12	5.60	3.39	0.25	0.49

ing models on Partial RSFC using PCA. All results were average model

evaluation scores calculated based on ten replications on the test dataset. The minimum, maximum, mean, and standard deviation scores were reported for each metric. The accuracy scores achieved by all the tested models on Partial RSFC using PCA ranges, on average, between 56.11%–60.69%. The proposed GRU exhibited a significantly higher accuracy ($60.69\% \pm 1.14\%$) than KSVC, LSVC, LR+SF_M, RFC, ABC, and LSTM models. The sensitivity scores obtained from KSVC, LSVC, LR+SF_M, RFC, ABC, LSTM and GRU on the dataset were 45.27%, 53.94%, 29.75%, 40.76%, 40.17%, 56.67% and 57.57%, respectively. Consistent with the accuracy results, GRU also had better sensitivity ($57.57\% \pm 1.31\%$) than all other compared models. While the specificity ($85.41\% \pm 5.12\%$) and AUC ($64.36\% \pm 5.12\%$) of the LR+SF_M were significantly higher than GRU, we noted that the LR+SF_M had a higher standard deviation simultaneously, suggesting that the results had a wider spread as compared to other methods. Moreover, the LR+SF_M method had a lower sensitivity ($29.75\% \pm 6.24\%$). Therefore, LR+SF_M did not achieve the best mean precision in our experiments. We also observed that the LSTM had the lowest standard deviation, among other approaches. However, the performance of LSTM was inferior to GRU in terms of accuracy, sensitivity, and AUC rates. Given the proposed GRU achieved an improved classification accuracy ($60.69\% \pm 1.14\%$), sensitivity ($57.57\% \pm 1.31\%$), specificity ($62.97\% \pm 1.88\%$), and AUC ($60.61\% \pm 1.88\%$) among compared machine learning models, and therefore the GRU had the highest precision, and the LSTM is the closest competitor.

Table 3 presents the average performance scores of the various supervised learning models on Pearson's RSFC using PCA. To assess the performance of various supervised learning models dealing with the ASD classification problem on Pearson's RSFC, the experiments using KSVC, LSVC, LR+SF_M, RFC, ABC, LSTM, and GRU, have been conducted. The final evaluations were determined concerning each approach's average accuracy, sensitivity, specificity, and AUC metrics. The two best performing approaches were LR+SF_M and GRU with the classification accuracies of $71.17\% \pm 4.92\%$ and $69.16\% \pm 1.45\%$, respectively. While the sensitivity of GRU ($69.47\% \pm 2.26\%$) was only slightly greater than LR+SF_M ($68.88\% \pm 7.81\%$), the lower standard deviation signified its highly stable performance on detecting ASD patients in comparison to LR+SF_M. Despite RFC having the highest specificity ($82.22\% \pm 5.38\%$), it also obtained, among other methods, the lowest sensitivity ($37.46\% \pm 8.43\%$), namely, it successfully identified the normal controls but overlooked actual ASD subjects significantly. LR+SF_M was superior to GRU by achieving a better AUC score of $77.38\% \pm 4.51\%$. However, LR+SF_M had higher standard deviations of the accuracy, sensitivity, specificity, and AUC scores, demonstrating its weak classification consistency. In general, the best performing method achieved an overall accuracy, sensitivity, specificity, and AUC scores of $69.16\% \pm 1.45\%$, $69.47\% \pm 2.26\%$, $69.47\% \pm 2.26\%$ and $74.15\% \pm 0.72\%$, using GRU approach based on Pearson's RSFC, and the

Table 3: Performance scores of the various supervised learning models on Pearson’s RSFC using PCA

Metrics	Methods	KSVC	LSVC	LR +SFM	RFC	ABC	LSTM	GRU
Accuracy	Min	56.32	47.13	60.92	47.73	54.02	64.00	67.16
	Average	67.27	62.08	71.17	62.04	60.10	67.42	69.16
	Max	79.31	73.56	86.36	78.16	68.57	70.29	71.37
	Std	4.92	4.79	4.92	4.87	3.19	2.19	1.45
Sensitivity	Min	40	42.50	52.50	19.51	30.86	56.41	66.37
	Average	60.77	60.47	68.88	37.46	41.27	62.69	69.47
	Max	77.50	77.50	85.37	57.50	54.30	67.95	71.68
	Std	8.53	7.70	7.81	8.43	5.36	4.11	2.26
Specificity	Min	59.57	38.30	61.70	67.39	66.67	67.01	67.11
	Average	72.86	63.46	73.14	82.22	76.32	71.24	68.93
	Max	85.11	78.26	89.36	95.74	89.25	75.26	71.14
	Std	5.78	7.09	5.68	5.38	4.87	2.89	1.34
AUC	Min	58.51	53.67	66.06	55	53.98	69.39	73.09
	Average	74.07	66.99	77.38	66.88	63.53	72.35	74.15
	Max	84.10	77.36	87.40	81.06	72.75	75.48	75.04
	Std	4.97	4.67	4.51	5.37	3.64	1.86	0.72

LR+SFM is the closest competitor.

To assess how our model behaves on Spearman’s RSFC using PCA, we observed the accuracy, sensitivity, specificity, and AUC metrics on the unseen data for each supervised learning model experimented. Table 4 presents the average performance scores of all the supervised learning models implemented on Spearman’s RSFC using PCA. In Table 4, we observed that the LR+SFM achieved a mean classification accuracy of $68.48\% \pm 4.14\%$ (sensitivity $65.58\% \pm 7.29\%$, specificity $70.98\% \pm 5.17\%$, and AUC $74.88\% \pm 4.67\%$), obtained from ten replications on the test dataset. While the RFC approach achieved a relatively low average accuracy of $61.48\% \pm 3.87\%$ (sensitivity $40.66\% \pm 6.35\%$, specificity $79.40\% \pm 5.15\%$, and AUC $67.39\% \pm 4.77\%$), it attained the highest specificity, illustrating its outstanding capability in accurately identifying control group. Meanwhile, the GRU classifier obtained a mean accuracy of $68.28\% \pm 1.58\%$ (sensitivity $67.80\% \pm 1.88\%$, specificity $68.71\% \pm 1.83\%$, and AUC $74.49\% \pm 1.17\%$). The result showed that the sensitivity of GRU was superior to the other six classifiers on the dataset; namely, GRU had the highest ability to designate an individual with the disease as positive, and thus fewer cases of the disease were missed. In addition, GRU had lower standard deviations in accuracy, sensitivity, specificity, and AUC, demonstrating its strong classification consistency. Thus, based upon

Table 4: Performance scores of the various supervised learning models on Spearman’s RSFC using PCA

Metrics	Methods	KSVC	LSVC	LR +SFM	RFC	ABC	LSTM	GRU
Accuracy	Min	56.32	48.28	56.32	51.72	53.14	64.57	66.03
	Average	67.41	61.83	68.48	61.48	60.69	66.17	68.28
	Max	79.31	72.41	78.16	70.11	67.82	70.29	70.61
	Std	5.06	4.72	4.14	3.87	2.95	1.74	1.58
Sensitivity	Min	40	45	48.78	25	34.57	58.97	64.23
	Average	60.97	59.69	65.58	40.66	45.21	62.69	67.80
	Max	80.49	77.50	82.93	55	55.56	69.23	71.22
	Std	7.70	7.07	7.29	6.35	4.97	3.22	1.88
Specificity	Min	56.52	46.81	53.19	65.22	63.44	65.98	65.47
	Average	72.94	63.66	70.98	79.40	74	68.99	68.71
	Max	86.96	80.85	82.98	89.36	84.04	73.20	71.22
	Std	6.88	7.13	5.71	5.15	4.71	2.09	1.83
AUC	Min	61.33	48.14	64.20	55.32	58.05	70.94	73.05
	Average	73.55	65.88	74.88	67.39	64.69	72.07	74.49
	Max	85.11	77.45	89.50	77.50	72.63	73.45	76.95
	Std	4.95	5.44	4.67	4.77	3.34	0.79	1.17

the results of Spearman’s RSFC, GRU was selected to generate classification systems that have better performance in terms of sensitivity, specificity, and accuracy among all the compared models.

From tables 2, 3, and 4, we observed that the average performance scores of the LR + SFM model on the Pearson’s RSFC using PCA is higher among all other compared methods. On the other hand, the popular deep learning methods GRU and LSTM have the closest scores with a lower variation. From the application point of view, the GRU model is more reliable and chosen as the best model, and the LSTM and LR + SFM model are the closest competitors. The results have some limitations from the inference perspective as the features are selected by applying PCA on the RSFCs. The most important brain regions to identify the ASD cannot be accurately determined as the features are the principal components which is the linear combination of the 19,900 original features.

5 Discussion and Conclusion

In this article, we classified autistic and normal patients using various supervised learning methods. The RSFC obtained from Pearson’s correlation,

Spearman's rank correlation, and the Partial correlation was used. The performance of the classification models corresponding to each rs-RSFC measure is compared using the accuracy, specificity, sensitivity, and roc AUC scores. Since the total number of observations is 871 and the number of features is 19,900, our model faces the curse of dimensionality, so the PCA was implemented for dimension reduction. The experiments are conducted on the original data and the data after implementing PCA. The application of PCA improves the model performance and significantly reduces the computational time at the cost of interpretability of features. The supervised learning methods LR, KSVC, LSVC, RFC, ABC, LSTM, and GRU, were implemented on the original and transformed data with PCA. LSTM and GRU model with various neurons value from 10 to 250 with a range of values of the hyperparameters is compared, and the simplest model with the best accuracy is chosen. Pearson's RSFC is considered a better measure of connectivity for the ASD classification as the highest performance scores are obtained on PCA-transformed Pearson's RSFC data. Although the LR model has overall higher average performance scores, this model has a high variance. The GRU model has slightly lower accuracy, specificity, and AUC scores and slightly higher sensitivity scores. However, the GRU model has a much smaller variance. So the GRU model is considered the best model and is chosen for the classification. The LSTM model remains competitive in model accuracy and sensitivity and has a consistent performance measure compared to other methods. For precision, our experiments suggest the GRU method to be preferable. The classification result on the original data is much worse with high computational cost in comparison to the PCA transformed data.

Our work has some limitations. The proposed model frameworks are less beneficial for the statistical inference point of view. Since the principal components are the linear combination of the original variables with corresponding weight values, it is difficult to identify which brain regions contribute more to classifying autistic and normal patients. Without the implementation of PCA, these methods can be utilized if inference is our main objective. In that case, we see a significant loss in precision. Also, as the sample size is small, the overall performance scores may depend on the split of the data set. In addition, the LSTM neural network expects to have a decent sample size to learn the value of the parameters. Therefore, the model performance may be improved with a larger data set. Exploring the hybrid classification techniques, implementing various global optimizers and local optimizers in the model, applying other dimension reduction techniques such as independent component analysis, autoencoders, and manifold learning methods is a matter of future work.

Acknowledgments. This research work is partially supported by MTSU FRCAC grant.

.1 Hyperparameter tuning for single layer LSTM on various RSFCs

Hyperparameter tuning for single layer LSTM on the Pearson's RSFC

Table 1: Hyperparameter tuning for 30 neurons single layer LSTM on the Pearson's RSFC.

Optimizer	Learning rate	Batch size			
		4	8	16	32
Adam	0.01	0.6179	0.6204	0.6174	0.6143
	0.005	0.6121	0.6117	0.6104	0.6118
	0.001	0.6111	0.6115	0.6123	0.6123
	0.0005	0.6126	0.6127	0.6130	0.6132
	0.0001	0.6132	0.6129	0.6130	0.6121
Nadam	0.01	0.6117	0.6127	0.6130	0.6131
	0.005	0.6137	0.6142	0.6151	0.6154
	0.001	0.6137	0.6119	0.6096	0.6076
	0.0005	0.6054	0.6033	0.6010	0.5988
	0.0001	0.5967	0.5943	0.5920	0.5897
Adagrad	0.01	0.5900	0.5905	0.5910	0.5913
	0.005	0.5920	0.5924	0.5927	0.5928
	0.001	0.5934	0.5938	0.5938	0.5941
	0.0005	0.5944	0.5949	0.5950	0.5954
	0.0001	0.5954	0.5956	0.5960	0.5966

Table 2: Hyperparameter tuning for 50 neurons single layer LSTM on the Pearson's RSFC.

Optimizer	Learning rate	Batch size			
		4	8	16	32
Adam	0.01	0.6286	0.6232	0.6210	0.6225
	0.005	0.6216	0.6207	0.6193	0.6190
	0.001	0.6186	0.6184	0.6171	0.6154
	0.0005	0.6163	0.6154	0.6162	0.6163
	0.0001	0.6176	0.6166	0.6166	0.6156
Nadam	0.01	0.6159	0.6160	0.6171	0.6176
	0.005	0.6183	0.6187	0.6188	0.6190
	0.001	0.6180	0.6171	0.6165	0.6141
	0.0005	0.6124	0.6109	0.6085	0.6064
	0.0001	0.6034	0.6006	0.5981	0.5955
Adagrad	0.01	0.5961	0.5966	0.5970	0.5972
	0.005	0.5975	0.5978	0.5979	0.5982
	0.001	0.5986	0.5990	0.5993	0.5997
	0.0005	0.5600	0.6002	0.6007	0.6011
	0.0001	0.6014	0.6016	0.6017	0.6020

Table 3: Hyperparameter tuning for 100 neurons single layer LSTM on the Pearson's RSFC.

Optimizer	Learning rate	Batch size			
		4	8	16	32
Adam	0.01	0.6129	0.6118	0.6139	0.6123
	0.005	0.6126	0.6131	0.6139	0.6142
	0.001	0.6144	0.6145	0.6151	0.6146
	0.0005	0.6152	0.6158	0.6166	0.6168
	0.0001	0.6161	0.6163	0.6165	0.6164
Nadam	0.01	0.6174	0.6181	0.6182	0.6186
	0.005	0.6194	0.6199	0.6208	0.6208
	0.001	0.6208	0.6201	0.6187	0.6173
	0.0005	0.6168	0.6160	0.6143	0.6123
	0.0001	0.6093	0.6065	0.6038	0.6014
Adagrad	0.01	0.6015	0.6019	0.6022	0.6023
	0.005	0.6027	0.6029	0.6032	0.6036
	0.001	0.6036	0.6038	0.6042	0.6045
	0.0005	0.6044	0.6048	0.6049	0.6051
	0.0001	0.6056	0.6058	0.6060	0.6062

Table 4: Hyperparameter tuning for 150 neurons single layer LSTM on the Pearson's RSFC.

Optimizer	Learning rate	Batch size			
		4	8	16	32
Adam	0.01	0.6121	0.6164	0.6167	0.6123
	0.005	0.6147	0.6151	0.6153	0.6163
	0.001	0.6167	0.6172	0.6173	0.6176
	0.0005	0.6187	0.6185	0.6185	0.6184
	0.0001	0.6185	0.6183	0.6177	0.6179
Nadam	0.01	0.6180	0.6186	0.6195	0.6199
	0.005	0.6201	0.6204	0.6207	0.6212
	0.001	0.6213	0.6218	0.6210	0.6195
	0.0005	0.6187	0.6176	0.6164	0.6144
	0.0001	0.6123	0.6101	0.6075	0.6049
Adagrad	0.01	0.6049	0.6052	0.6053	0.6056
	0.005	0.6059	0.6060	0.6062	0.6064
	0.001	0.6066	0.6067	0.6070	0.6071
	0.0005	0.6072	0.6073	0.6076	0.6083
	0.0001	0.6084	0.6085	0.6086	0.6089

Table 5: Hyperparameter tuning for 200 neurons single layer LSTM on the Pearson's RSFC.

Optimizer	Learning rate	Batch size			
		4	8	16	32
Adam	0.01	0.6121	0.6236	0.6240	0.6230
	0.005	0.6234	0.6223	0.6233	0.6251
	0.001	0.6252	0.6244	0.6256	0.6267
	0.0005	0.6274	0.6283	0.6295	0.6292
	0.0001	0.6301	0.6305	0.6318	0.6323
Nadam	0.01	0.6327	0.6337	0.6347	0.6351
	0.005	0.6356	0.6362	0.6371	0.6378
	0.001	0.6383	0.6393	0.6389	0.6377
	0.0005	0.6375	0.6366	0.6356	0.6332
	0.0001	0.6300	0.6273	0.6244	0.6221
Adagrad	0.01	0.6218	0.6219	0.6219	0.6219
	0.005	0.6218	0.6220	0.6222	0.6222
	0.001	0.6223	0.6227	0.6230	0.6231
	0.0005	0.6232	0.6234	0.6235	0.6238
	0.0001	0.6240	0.6245	0.6246	0.6251

Table 6: Hyperparameter tuning for 250 neurons single layer LSTM on the Pearson's RSFC.

Optimizer	Learning rate	Batch size			
		4	8	16	32
Adam	0.01	0.6271	0.6254	0.6264	0.6264
	0.005	0.6260	0.6265	0.6263	0.6265
	0.001	0.6261	0.6262	0.6260	0.6270
	0.0005	0.6276	0.6283	0.6280	0.6283
	0.0001	0.6299	0.6300	0.6307	0.6311
Nadam	0.01	0.6325	0.6339	0.6348	0.6354
	0.005	0.6362	0.6373	0.6380	0.6384
	0.001	0.6390	0.6394	0.6397	0.6382
	0.0005	0.6384	0.6376	0.6366	0.6346
	0.0001	0.6312	0.6284	0.6266	0.6233
Adagrad	0.01	0.6229	0.6224	0.6224	0.6221
	0.005	0.6219	0.6220	0.6219	0.6219
	0.001	0.6219	0.6219	0.6222	0.6225
	0.0005	0.6228	0.6231	0.6233	0.6233
	0.0001	0.6237	0.6241	0.6245	0.6248

Hyperparameter tuning for single layer LSTM on the Partial Correlation RSFC

Table 7: Hyperparameter tuning for 10 neurons single layer LSTM on the Partial Corr RSFC.

Optimizer	Learning rate	Batch size			
		4	8	16	32
Adam	0.01	0.5421	0.5475	0.5514	0.5536
	0.005	0.5537	0.5538	0.5540	0.5543
	0.001	0.5553	0.5556	0.5555	0.5558
	0.0005	0.5571	0.5573	0.5566	0.5547
	0.0001	0.5546	0.5540	0.5538	0.5521
Nadam	0.01	0.5519	0.5518	0.5518	0.5512
	0.005	0.5523	0.5516	0.5507	0.5487
	0.001	0.5475	0.5457	0.5444	0.5424
	0.0005	0.5410	0.5404	0.5393	0.5378
	0.0001	0.5369	0.5361	0.5350	0.5342
Adagrad	0.01	0.5347	0.5349	0.5353	0.5356
	0.005	0.5359	0.5366	0.5368	0.5373
	0.001	0.5380	0.5388	0.5393	0.5392
	0.0005	0.5396	0.5398	0.5398	0.5399
	0.0001	0.5399	0.5401	0.5402	0.5402

Table 8: Hyperparameter tuning for 30 neurons single layer LSTM on the Partial Corr RSFC.

Optimizer	Learning rate	Batch size			
		4	8	16	32
Adam	0.01	0.5478	0.5568	0.5550	0.5539
	0.005	0.5523	0.5527	0.5543	0.5537
	0.001	0.5551	0.5567	0.5560	0.5574
	0.0005	0.5581	0.5590	0.5583	0.5570
	0.0001	0.5575	0.5577	0.5575	0.5569
Nadam	0.01	0.5569	0.5572	0.5571	0.5567
	0.005	0.5576	0.5570	0.5558	0.5544
	0.001	0.5530	0.5516	0.5501	0.5484
	0.0005	0.5473	0.5457	0.5444	0.5431
	0.0001	0.5417	0.5406	0.5395	0.5382
Adagrad	0.01	0.5383	0.5388	0.5392	0.5393
	0.005	0.5397	0.5399	0.5403	0.5407
	0.001	0.5414	0.5420	0.5424	0.5427
	0.0005	0.5433	0.5438	0.5441	0.5442
	0.0001	0.5446	0.5448	0.5447	0.5446

Table 9: Hyperparameter tuning for 50 neurons single layer LSTM on the Partial Corr RSFC.

Optimizer	Learning rate	Batch size			
		4	8	16	32
Adam	0.01	0.5643	0.5575	0.5536	0.5543
	0.005	0.5520	0.5542	0.5540	0.5542
	0.001	0.5552	0.5572	0.5579	0.5585
	0.0005	0.5597	0.5612	0.5611	0.5600
	0.0001	0.5601	0.5607	0.5602	0.5589
Nadam	0.01	0.5586	0.5588	0.5590	0.5585
	0.005	0.5588	0.5587	0.5580	0.5556
	0.001	0.5544	0.5527	0.5514	0.5499
	0.0005	0.5486	0.5475	0.5457	0.5442
	0.0001	0.5427	0.5419	0.5408	0.5396
Adagrad	0.01	0.5400	0.5404	0.5405	0.5406
	0.005	0.5408	0.5411	0.5415	0.5418
	0.001	0.5424	0.5431	0.5434	0.5438
	0.0005	0.5444	0.5451	0.5455	0.5456
	0.0001	0.5462	0.5465	0.5466	0.5465

Table 10: Hyperparameter tuning for 100 neurons single layer LSTM on the Partial Corr RSFC.

Optimizer	Learning rate	Batch size			
		4	8	16	32
Adam	0.01	0.5486	0.5493	0.5543	0.5546
	0.005	0.5567	0.5562	0.5561	0.5559
	0.001	0.5563	0.5574	0.5581	0.5579
	0.0005	0.5592	0.5607	0.5613	0.5615
	0.0001	0.5618	0.5625	0.5631	0.5626
Nadam	0.01	0.5632	0.5632	0.5628	0.5623
	0.005	0.5627	0.5621	0.5614	0.5600
	0.001	0.5581	0.5574	0.5554	0.5541
	0.0005	0.5533	0.5523	0.5513	0.5502
	0.0001	0.5490	0.5479	0.5466	0.5452
Adagrad	0.01	0.5453	0.5459	0.5458	0.5457
	0.005	0.5462	0.5465	0.5464	0.5465
	0.001	0.5468	0.5473	0.5476	0.5479
	0.0005	0.5483	0.5488	0.5492	0.5493
	0.0001	0.5497	0.5501	0.5502	0.5501

Table 11: Hyperparameter tuning for 150 neurons single layer LSTM on the Partial Corr RSFC.

Optimizer	Learning rate	Batch size			
		4	8	16	32
Adam	0.01	0.5543	0.5575	0.5569	0.5577
	0.005	0.5591	0.5607	0.5610	0.5617
	0.001	0.5621	0.5627	0.5623	0.5639
	0.0005	0.5649	0.5661	0.5665	0.5669
	0.0001	0.5674	0.5675	0.5672	0.5668
Nadam	0.01	0.5672	0.5668	0.5668	0.5658
	0.005	0.5665	0.5657	0.5644	0.5623
	0.001	0.5621	0.5605	0.5603	0.5583
	0.0005	0.5576	0.5569	0.5560	0.5540
	0.0001	0.5526	0.5514	0.5499	0.5485
Adagrad	0.01	0.5486	0.5487	0.5490	0.5490
	0.005	0.5492	0.5494	0.5496	0.5497
	0.001	0.5502	0.5503	0.5504	0.5506
	0.0005	0.5511	0.5516	0.5520	0.5519
	0.0001	0.5522	0.5524	0.5528	0.5528

Table 12: Hyperparameter tuning for 200 neurons single layer LSTM on the Partial Corr RSFC.

Optimizer	Learning rate	Batch size			
		4	8	16	32
Adam	0.01	0.5650	0.5643	0.5626	0.5602
	0.005	0.5604	0.5589	0.5590	0.5590
	0.001	0.5697	0.5608	0.5614	0.5619
	0.0005	0.5636	0.5637	0.5641	0.5639
	0.0001	0.5646	0.5646	0.5644	0.5638
Nadam	0.01	0.5641	0.5645	0.5654	0.5642
	0.005	0.5642	0.5642	0.5637	0.5620
	0.001	0.5606	0.5599	0.5581	0.5562
	0.0005	0.5551	0.5533	0.5521	0.5507
	0.0001	0.5493	0.5481	0.5469	0.5455
Adagrad	0.01	0.5456	0.5461	0.5463	0.5466
	0.005	0.5467	0.5471	0.5474	0.5475
	0.001	0.5478	0.5484	0.5489	0.5490
	0.0005	0.5495	0.5501	0.5505	0.5508
	0.0001	0.5515	0.5518	0.5520	0.5519

Table 13: Hyperparameter tuning for 250 neurons single layer LSTM on the Partial Corr RSFC.

Optimizer	Learning rate	Batch size			
		4	8	16	32
Adam	0.01	0.5457	0.5493	0.5524	0.5543
	0.005	0.5536	0.5551	0.5569	0.5565
	0.001	0.5574	0.5589	0.5593	0.5589
	0.0005	0.5600	0.5608	0.5604	0.5605
	0.0001	0.5619	0.5630	0.5626	0.5627
Nadam	0.01	0.5635	0.5646	0.5646	0.5644
	0.005	0.5643	0.5643	0.5642	0.5627
	0.001	0.5618	0.5605	0.5586	0.5563
	0.0005	0.5551	0.5535	0.5519	0.5510
	0.0001	0.5494	0.5481	0.5468	0.5454
Adagrad	0.01	0.5459	0.5462	0.5463	0.5467
	0.005	0.5469	0.5470	0.5473	0.5475
	0.001	0.5477	0.5480	0.5484	0.5485
	0.0005	0.5489	0.5492	0.5493	0.5495
	0.0001	0.5500	0.5505	0.5509	0.5510

Hyperparameter tuning for single layer LSTM on the Spearman's RSFC

Table 14: Hyperparameter tuning for 10 neurons single layer LSTM on the Spearman's RSFC.

Optimizer	Learning rate	Batch size			
		4	8	16	32
Adam	0.01	0.6271	0.6314	0.6424	0.6443
	0.005	0.6427	0.6433	0.6431	0.6441
	0.001	0.6445	0.6442	0.6444	0.6424
	0.0005	0.6426	0.6423	0.6420	0.6422
	0.0001	0.6416	0.6406	0.6398	0.6381
Nadam	0.01	0.6372	0.6373	0.6376	0.6380
	0.005	0.6372	0.6377	0.6374	0.6365
	0.001	0.6353	0.6334	0.6309	0.6284
	0.0005	0.6256	0.6231	0.6200	0.6171
	0.0001	0.6139	0.6104	0.6072	0.6048
Adagrad	0.01	0.6056	0.6066	0.6075	0.6085
	0.005	0.6093	0.6100	0.6110	0.6118
	0.001	0.6125	0.6128	0.6134	0.6141
	0.0005	0.6150	0.6156	0.6159	0.6162
	0.0001	0.6163	0.6167	0.6171	0.6172

Table 15: Hyperparameter tuning for 30 neurons single layer LSTM on the Spearman's RSFC.

Optimizer	Learning rate	Batch size			
		4	8	16	32
Adam	0.01	0.6286	0.6428	0.6505	0.6504
	0.005	0.6523	0.6529	0.6527	0.6522
	0.001	0.6524	0.6529	0.6528	0.6532
	0.0005	0.6530	0.6539	0.6536	0.6538
	0.0001	0.6527	0.6517	0.6512	0.6508
Nadam	0.01	0.6505	0.6502	0.6493	0.6490
	0.005	0.6486	0.6477	0.6471	0.6461
	0.001	0.6446	0.6432	0.6412	0.6388
	0.0005	0.6366	0.6245	0.6317	0.6288
	0.0001	0.6265	0.6235	0.6205	0.6175
Adagrad	0.01	0.6180	0.6184	0.6196	0.6201
	0.005	0.6207	0.6216	0.6225	0.6234
	0.001	0.6240	0.6243	0.6248	0.6253
	0.0005	0.6257	0.6261	0.6267	0.6271
	0.0001	0.6275	0.6273	0.6275	0.6278

Table 16: Hyperparameter tuning for 50 neurons single layer LSTM on the Spearman's RSFC.

Optimizer	Learning rate	Batch size			
		4	8	16	32
Adam	0.01	0.6493	0.6532	0.6626	0.6636
	0.005	0.6641	0.6634	0.6639	0.6635
	0.001	0.6635	0.6629	0.6619	0.6603
	0.0005	0.6597	0.6586	0.6582	0.6571
	0.0001	0.6565	0.6562	0.6552	0.6545
Nadam	0.01	0.6540	0.6534	0.6425	0.6516
	0.005	0.6509	0.6502	0.6497	0.6489
	0.001	0.6482	0.6475	0.6456	0.6435
	0.0005	0.6414	0.6391	0.6368	0.6337
	0.0001	0.6307	0.6270	0.6242	0.6211
Adagrad	0.01	0.6217	0.6225	0.6234	0.6245
	0.005	0.6256	0.6264	0.6270	0.6275
	0.001	0.6283	0.6290	0.6293	0.6296
	0.0005	0.6303	0.6305	0.6308	0.6312
	0.0001	0.6315	0.6319	0.6324	0.6326

Table 17: Hyperparameter tuning for 100 neurons single layer LSTM on the Spearman's RSFC.

Optimizer	Learning rate	Batch size			
		4	8	16	32
Adam	0.01	0.6621	0.6536	0.6505	0.6532
	0.005	0.6524	0.6557	0.6578	0.6571
	0.001	0.6585	0.6591	0.6598	0.6601
	0.0005	0.6605	0.6611	0.6620	0.6615
	0.0001	0.6601	0.6604	0.6605	0.6592
Nadam	0.01	0.6586	0.6574	0.6563	0.6551
	0.005	0.6543	0.6535	0.6524	0.6519
	0.001	0.6510	0.6499	0.6481	0.6468
	0.0005	0.6454	0.6446	0.6424	0.6404
	0.0001	0.6377	0.6346	0.6327	0.6296
Adagrad	0.01	0.6300	0.6306	0.6312	0.6318
	0.005	0.6326	0.6331	0.6336	0.6341
	0.001	0.6350	0.6353	0.6360	0.6365
	0.0005	0.6369	0.6372	0.6376	0.6379
	0.0001	0.6383	0.6386	0.6387	0.6388

Table 18: Hyperparameter tuning for 150 neurons single layer LSTM on the Spearman's RSFC.

Optimizer	Learning rate	Batch size			
		4	8	16	32
Adam	0.01	0.6336	0.6343	0.6374	0.6359
	0.005	0.6364	0.6363	0.6361	0.6361
	0.001	0.6379	0.6406	0.6417	0.6419
	0.0005	0.6427	0.6433	0.6437	0.6442
	0.0001	0.6447	0.6453	0.6454	0.6460
Nadam	0.01	0.6462	0.6460	0.6465	0.6468
	0.005	0.6473	0.6475	0.6472	0.6470
	0.001	0.6471	0.6470	0.6463	0.6452
	0.0005	0.6446	0.6434	0.6416	0.6391
	0.0001	0.6365	0.6341	0.6315	0.6282
Adagrad	0.01	0.6282	0.6285	0.6288	0.6290
	0.005	0.6293	0.6294	0.6298	0.6302
	0.001	0.6309	0.6312	0.6314	0.6318
	0.0005	0.6322	0.6326	0.6329	0.6333
	0.0001	0.6337	0.6340	0.6341	0.6345

Table 19: Hyperparameter tuning for 200 neurons single layer LSTM on the Spearman's RSFC.

Optimizer	Learning rate	Batch size			
		4	8	16	32
Adam	0.01	0.6279	0.6354	0.6345	0.6348
	0.005	0.6347	0.6361	0.6360	0.6382
	0.001	0.6397	0.6402	0.6416	0.6420
	0.0005	0.6432	0.6434	0.6443	0.6451
	0.0001	0.6462	0.6466	0.6469	0.6470
Nadam	0.01	0.6471	0.6478	0.6484	0.6484
	0.005	0.6481	0.6485	0.6483	0.6486
	0.001	0.6491	0.6493	0.6490	0.6477
	0.0005	0.6478	0.6472	0.6459	0.6439
	0.0001	0.6410	0.6382	0.6350	0.6323
Adagrad	0.01	0.6324	0.6323	0.6330	0.6331
	0.005	0.6330	0.6331	0.6335	0.6340
	0.001	0.6342	0.6346	0.6349	0.6351
	0.0005	0.6353	0.6357	0.6361	0.6363
	0.0001	0.6367	0.6371	0.6372	0.6375

Table 20: Hyperparameter tuning for 250 neurons single layer LSTM on the Spearman's RSFC.

Optimizer	Learning rate	Batch size			
		4	8	16	32
Adam	0.01	0.6400	0.6379	0.6379	0.6391
	0.005	0.6377	0.6362	0.6376	0.6377
	0.001	0.6390	0.6411	0.6425	0.6425
	0.0005	0.6436	0.6447	0.6446	0.6450
	0.0001	0.6453	0.6454	0.6456	0.6459
Nadam	0.01	0.6467	0.6468	0.6472	0.6479
	0.005	0.6478	0.6485	0.6479	0.6480
	0.001	0.6484	0.6489	0.6487	0.6476
	0.0005	0.6476	0.6475	0.6462	0.6443
	0.0001	0.6417	0.6391	0.6366	0.6336
Adagrad	0.01	0.6335	0.6334	0.6337	0.6337
	0.005	0.6339	0.6341	0.6341	0.6345
	0.001	0.6348	0.6350	0.6355	0.6359
	0.0005	0.6364	0.6367	0.6371	0.6375
	0.0001	0.6376	0.6378	0.6381	0.6384

.2 Hyperparameter tuning for single layer GRU with various RSFCs

Hyperparameter tuning for single layer GRU on the Pearson's RSFC

Table 21: Hyperparameter tuning for 10 neurons single layer GRU with Pearson's RSFC.

Optimizer	Learning rate	Batch size			
		4	8	16	32
Adam	0.01	0.6085	0.6160	0.6169	0.6155
	0.001	0.6161	0.6145	0.6144	0.6134
	0.0005	0.6129	0.6134	0.6145	0.6152
	0.0001	0.6163	0.6171	0.6165	0.6152
Nadam	0.01	0.6150	0.6158	0.6156	0.6167
	0.001	0.6141	0.6111	0.6092	0.6058
	0.0005	0.6017	0.5994	0.5966	0.5934
	0.0001	0.5986	0.5879	0.5848	0.5823
Adagrad	0.01	0.5829	0.5836	0.5843	0.5854
	0.001	0.5862	0.5870	0.5878	0.5886
	0.0005	0.5891	0.5899	0.5905	0.5913
	0.0001	0.5921	0.5923	0.5926	0.5921

Table 22: Hyperparameter tuning for 30 neurons single layer GRU with Pearson's RSFC.

Optimizer	Learning rate	Batch size			
		4	8	16	32
Adam	0.01	0.6029	0.6132	0.6160	0.6170
	0.001	0.6186	0.6188	0.6187	0.6199
	0.0005	0.6209	0.6204	0.6214	0.6213
	0.0001	0.6217	0.6215	0.6210	0.6202
Nadam	0.01	0.6205	0.6206	0.6202	0.6191
	0.001	0.6182	0.6167	0.6152	0.6125
	0.0005	0.6104	0.6081	0.6059	0.6028
	0.0001	0.5994	0.5965	0.5939	0.5912
Adagrad	0.01	0.5916	0.5923	0.5930	0.5936
	0.001	0.5945	0.5951	0.5957	0.5964
	0.0005	0.5967	0.5974	0.5980	0.5985
	0.0001	0.5993	0.5999	0.6003	0.6004

Table 23: Hyperparameter tuning for 50 neurons single layer GRU with Pearson's RSFC.

Optimizer	Learning rate	Batch size			
		4	8	16	32
Adam	0.01	0.6107	0.6125	0.6174	0.6152
	0.001	0.6187	0.62	0.62	0.6208
	0.0005	0.6216	0.6221	0.6232	0.6227
	0.0001	0.6229	0.6220	0.6222	0.6233
Nadam	0.01	0.6234	0.6230	0.6229	0.6230
	0.001	0.6224	0.6209	0.6192	0.6174
	0.0005	0.616	0.6143	0.6120	0.6093
	0.0001	0.6064	0.6030	0.5999	0.5970
Adagrad	0.01	0.5977	0.5984	0.5988	0.5992
	0.001	0.5999	0.6006	0.6013	0.6018
	0.0005	0.6023	0.6028	0.6032	0.6038
	0.0001	0.6044	0.6051	0.6056	0.6058

Table 24: Hyperparameter tuning for 100 neurons single layer GRU with Pearson's RSFC.

Optimizer	Learning rate	Batch size			
		4	8	16	32
Adam	0.01	0.6157	0.6154	0.6114	0.6093
	0.001	0.6129	0.6146	0.6155	0.6159
	0.0005	0.6175	0.6188	0.6190	0.6189
	0.0001	0.6195	0.6198	0.6196	0.6197
Nadam	0.01	0.6204	0.6208	0.6213	0.6211
	0.001	0.6207	0.6200	0.6194	0.6183
	0.0005	0.6171	0.6148	0.6132	0.6110
	0.0001	0.6086	0.6055	0.6023	0.5997
Adagrad	0.01	0.6000	0.6009	0.6013	0.6018
	0.001	0.6022	0.6025	0.6030	0.6036
	0.0005	0.6040	0.6046	0.6050	0.6054
	0.0001	0.6060	0.6064	0.6064	0.6066

Table 25: Hyperparameter tuning for 150 neurons single layer GRU with Pearson's RSFC.

Optimizer	Learning rate	Batch size			
		4	8	16	32
Adam	0.01	0.6193	0.6179	0.6140	0.6104
	0.001	0.6129	0.6157	0.6169	0.6167
	0.0005	0.6181	0.6181	0.6188	0.6198
	0.0001	0.6197	0.62	0.6199	0.6212
Nadam	0.01	0.6213	0.6215	0.6213	0.6205
	0.001	0.6213	0.6222	0.6216	0.6201
	0.0005	0.6194	0.6180	0.6176	0.6157
	0.0001	0.6132	0.6101	0.6073	0.6035
Adagrad	0.01	0.6036	0.6038	0.6046	0.6049
	0.001	0.6056	0.6064	0.6068	0.6071
	0.0005	0.6077	0.6081	0.6083	0.6087
	0.0001	0.6088	0.6091	0.6093	0.6097

Table 26: Hyperparameter tuning for 200 neurons single layer GRU with Pearson's RSFC.

Optimizer	Learning rate	Batch size			
		4	8	16	32
Adam	0.01	0. 6114	0. . 6168	0. 6186	0. 6145
	0.001	0. 6191	0. 6202	0. 6208	0. 6221
	0.0005	0. 6231	0. 6246	0. 6242	0. 6242
	0.0001	0. 6242	0. 6236	0. 6236	0. 6229
Nadam	0.01	0. 6227	0. 6227	0. 6223	0. 6217
	0.001	0. 6222	0. 6224	0. 6209	0. 6207
	0.0005	0. 6206	0. 6194	0. 6178	0. 6173
	0.0001	0. 6146	0. 6111	0. 6081	0. 6052
Adagrad	0.01	0. 6055	0. 6058	0. 6060	0. 6063
	0.001	0. 6071	0. 6077	0. 6081	0. 6086
	0.0005	0. 6092	0. 6098	0. 6102	0. 6106
	0.0001	0. 6120	0. 6111	0. 6115	0. 6115

Table 27: Hyperparameter tuning for 250 neurons single layer GRU with Pearson's RSFC.

Optimizer	Learning rate	Batch size			
		4	8	16	32
Adam	0.01	0. 6193	0. 6168	0. 6176	0. 6171
	0.001	0. 6191	0. 6218	0. 6216	0. 6221
	0.0005	0. 6230	0. 6236	0. 6242	0. 6242
	0.0001	0. 6242	0. 6241	0. 6234	0. 6230
Nadam	0.01	0. 6235	0. 6236	0. 6229	0. 6235
	0.001	0. 6233	0. 6244	0. 6245	0. 6233
	0.0005	0. 6240	0. 6235	0. 6227	0. 6204
	0.0001	0. 6184	0. 6157	0. 6132	0. 6101
Adagrad	0.01	0. 6111	0. 6116	0. 6123	0. 6127
	0.001	0. 6132	0. 6138	0. 6142	0. 6144
	0.0005	0. 6146	0. 6148	0. 6152	0. 6155
	0.0001	0. 6156	0. 6156	0. 6160	0. 6160

Hyperparameter tuning for single layer GRU on the Spearman's RSFC

Table 28: Hyperparameter tuning for 10 neurons single layer GRU with Spearman's RSFC.

Optimizer	Learning rate	Batch size		
		4	8	16
Adam	0.01	0. 6236	0. 6225	0. 6229
	0.001	0. 6211	0. 6226	0. 6230
	0.0005	0. 6215	0. 6220	0. 6214
	0.0001	0. 6212	0. 6207	0. 6187
Nadam	0.01	0. 6197	0. 6209	0. 6206
	0.001	0. 6174	0. 6137	0. 6112
	0.0005	0. 6062	0. 6021	0. 5981
	0.0001	0. 5947	0. 5907	0. 5870
Adagrad	0.01	0. 5889	0. 5902	0. 5913
	0.001	0. 5924	0. 5936	0.5946
	0.0005	0. 5953	0. 5962	0. 5968
	0.0001	0. 5981	0. 5988	0. 5990

Table 29: Hyperparameter tuning for 30 neurons single layer GRU with Spearmans RSFC.

Optimizer	Learning rate	Batch size		
		4	8	16
Adam	0.01	0. 6193	0. 6254	0. 6271
	0.001	0. 6254	0. 625	0. 6254
	0.0005	0. 6261	0. 6253	0. 6249
	0.0001	0. 6272	0. 6272	0. 6265
Nadam	0.01	0. 6261	0. 6256	0. 6259
	0.001	0. 6240	0. 6218	0. 6199
	0.0005	0. 6169	0. 6133	0. 6095
	0.0001	0. 6056	0. 6007	0. 5966
Adagrad	0.01	0. 5979	0. 5983	0. 5994
	0.001	0. 6003	0. 6011	0. 6017
	0.0005	0. 6029	0. 6038	0. 6044
	0.0001	0. 6051	0. 6058	0. 6064

Table 30: Hyperparameter tuning for 50 neurons single layer GRU with Spearmans RSFC.

Optimizer	Learning rate	Batch size		
		4	8	16
Adam	0.01	0. 6164	0. 6214	0. 6212
	0.001	0. 6230	0. 6219	0. 6227
	0.0005	0. 6224	0. 6219	0. 6213
	0.0001	0. 6219	0. 6223	0. 6229
Nadam	0.01	0. 6235	0. 6244	0. 6252
	0.001	0. 6241	0. 6218	0. 6194
	0.0005	0. 6161	0. 6136	0. 6121
	0.0001	0. 6080	0. 6043	0. 6009
Adagrad	0.01	0. 6019	0. 6024	0. 6034
	0.001	0. 6043	0. 6050	0. 6055
	0.0005	0. 6059	0. 6063	0. 6065
	0.0001	0. 6071	0. 6076	0. 6084

Table 31: Hyperparameter tuning for 100 neurons single layer GRU with Spearmans RSFC.

Optimizer	Learning rate	Batch size		
		4	8	16
Adam	0.01	0. 6286	0. 6264	0. 6295
	0.001	0. 6266	0. 6251	0. 6258
	0.0005	0. 6259	0. 6253	0. 6248
	0.0001	0. 6243	0. 6232	0. 6240
Nadam	0.01	0. 6242	0. 6246	0. 625
	0.001	0. 6236	0. 6235	0. 6217
	0.0005	0. 6193	0. 6171	0. 6143
	0.0001	0. 6096	0. 6060	0. 6026
Adagrad	0.01	0. 6035	0. 6041	0. 6049
	0.001	0. 6057	0. 6061	0. 6064
	0.0005	0. 6075	0. 6077	0. 6084
	0.0001	0. 6088	0. 6092	0. 6096

Table 32: Hyperparameter tuning for 150 neurons single layer GRU with Spearmans RSFC.

Optimizer	Learning rate	Batch size		
		4	8	16
Adam	0.01	0. 6314	0. 6304	0. 6295
	0.001	0. 6282	0. 6267	0. 6246
	0.0005	0. 6234	0. 6228	0. 6235
	0.0001	0. 6238	0. 6239	0. 6249
Nadam	0.01	0. 6252	0. 6253	0. 6251
	0.001	0. 6254	0. 6262	0. 6268
	0.0005	0. 6256	0. 6250	0. 6230
	0.0001	0. 6192	0. 6150	0. 6120
Adagrad	0.01	0. 6123	0. 6130	0. 6136
	0.001	0. 6139	0. 6139	0. 6141
	0.0005	0. 6144	0. 6146	0. 6150
	0.0001	0. 6154	0. 6154	0. 6159

Table 33: Hyperparameter tuning for 200 neurons single layer GRU with Spearmans RSFC.

Optimizer	Learning rate	Batch size		
		4	8	16
Adam	0.01	0. 6379	0. 6421	0. 6336
	0.001	0. 6284	0. 6273	0. 6263
	0.0005	0. 6251	0. 6238	0. 6229
	0.0001	0. 6224	0. 6229	0. 6223
Nadam	0.01	0. 6224	0. 6230	0. 6223
	0.001	0. 6231	0. 6238	0. 6237
	0.0005	0. 6241	0. 6232	0. 6215
	0.0001	0. 6176	0. 6143	0. 6112
Adagrad	0.01	0. 6121	0. 6127	0. 6131
	0.001	0. 6134	0. 6136	0. 6140
	0.0005	0. 6141	0. 6143	0. 6146
	0.0001	0. 6149	0. 6150	0. 6154

Table 34: Hyperparameter tuning for 250 neurons single layer GRU with Spearmans RSFC.

Optimizer	Learning rate	Batch size		
		4	8	16
Adam	0.01	0. 6250	0. 6289	0. 6252
	0.001	0. 6213	0. 6191	0. 6183
	0.0005	0. 6191	0. 6181	0. 6183
	0.0001	0. 6186	0. 6179	0. 6190
Nadam	0.01	0. 6193	0. 6193	0. 6202
	0.001	0. 6209	0. 6210	0. 6206
	0.0005	0. 6215	0. 6219	0. 6206
	0.0001	0. 6171	0. 6144	0. 6114
Adagrad	0.01	0. 6122	0. 6122	0. 6131
	0.001	0. 6130	0. 6133	0. 6134
	0.0005	0. 6133	0. 6133	0. 6136
	0.0001	0. 6138	0. 6140	0. 6143

Hyperparameter tuning for single layer GRU on the Partial Correlation's RSFC

Table 35: Hyperparameter tuning for 10 neurons single layer GRU with Partial RSFC.

Optimizer	Learning rate	Batch size		
		4	8	16
Adam	0.01	0. 5271	0. 5282	0. 5283
	0.001	0. 5345	0. 5409	0. 5424
	0.0001	0. 5453	0.5468	0. 5459
Nadam	0.01	0. 5459	0. 5463	0. 5463
	0.001	0. 5449	0. 5438	0. 5436
	0.0001	0. 5415	0. 5393	0. 5373
Adagrad	0.01	0. 5371	0. 5368	0. 5365
	0.001	0. 5373	0. 5385	0. 5393
	0.0001	0. 5389	0. 5394	0. 5395
	0.0001	0. 5389	0. 5394	0. 5395

Table 36: Hyperparameter tuning for 30 neurons single layer GRU with Partial RSFC.

Optimizer	Learning rate	Batch size		
		4	8	16
Adam	0.01	0. 5171	0. 5186	0. 5186
	0.001	0. 5257	0. 5317	0. 5356
	0.0001	0. 5382	0. 5385	0. 5420
Nadam	0.01	0. 5446	0. 5458	0. 5463
	0.001	0. 5459	0. 5453	0. 5441
	0.0001	0. 5428	0. 5424	0. 5394
Adagrad	0.01	0. 5385	0. 5377	0. 5366
	0.001	0. 5371	0. 5376	0. 5380
	0.0001	0. 5389	0. 5392	0. 5401
	0.0001	0. 5389	0. 5392	0. 5401

References

- [1] Bowman, F.: Brain imaging analysis. Annual review of statistics and its application **1**, 61–8 (2014)

Table 37: Hyperparameter tuning for 50 neurons single layer GRU with Partial RSFC.

Optimizer	Learning rate	Batch size		
		4	8	16
Adam	0.01	0. 5321	0. 5300	0. 5267
	0.001	0. 5323	0. 5369	0. 54012
	0.0001	0. 5420	0. 5432	0. 5429
Nadam	0.01	0. 5446	0. 5465	0. 5483
	0.001	0. 5476	0. 5470	0. 5468
	0.0001	0. 5439	0. 5418	0. 5388
Adagrad	0.01	0. 5386	0. 5380	0. 5371
	0.001	0. 5377	0. 5384	0. 5393
	0.0001	0. 5403	0. 5412	0. 5413

Table 38: Hyperparameter tuning for 100 neurons single layer GRU with Partial RSFC.

Optimizer	Learning rate	Batch size		
		4	8	16
Adam	0.01	0. 5343	0. 5314	0. 5321
	0.001	0. 5371	0. 538	0. 5392
	0.0001	0. 5431	0. 5443	0. 5435
Nadam	0.01	0. 5447	0. 5460	0. 5473
	0.001	0. 5471	0. 5466	0. 5457
	0.0001	0. 5425	0. 5416	0. 5396
Adagrad	0.01	0. 5389	0. 5387	0. 5374
	0.001	0. 5380	0. 5383	0. 5388
	0.0001	0. 5399	0. 5408	0. 5408

- [2] Thabtah, F., Kamalov, F., Rajab, K.: A new computational intelligence approach to detect autistic features for autism screening. *International journal of medical informatics* **117**, 112–124 (2018)
- [3] Lord, C., Elsabbagh, M., Baird, G., Veenstra-Vanderweele, J.: Autism spectrum disorder. *The Lancet* **392**(10146), 508–520 (2018)
- [4] Khosla, M., Jamison, K., Ngo, G.H., Kuceyeski, A., Sabuncu, M.R.: Machine learning in resting-state fmri analysis. *Magnetic resonance imaging* **64**, 101–121 (2019)

Table 39: Hyperparameter tuning for 150 neurons single layer GRU with Partial RSFC.

Optimizer	Learning rate	Batch size		
		4	8	16
Adam	0.01	0. 5393	0. 53	0. 5279
	0.001	0. 5320	0. 5360	0. 5389
	0.0001	0. 5390	0. 5409	0. 5422
Nadam	0.01	0. 5432	0. 5442	0. 5454
	0.001	0. 5451	0. 5456	0. 5447
Adagrad	0.0001	0. 5424	0. 5411	0. 5385
	0.01	0. 5382	0. 5375	0. 5370
	0.001	0. 5377	0. 5382	0. 5388
	0.0001	0. 5393	0. 5396	0. 5397

Table 40: Hyperparameter tuning for 200 neurons single layer GRU with Partial RSFC.

Optimizer	Learning rate	Batch size		
		4	8	16
Adam	0.01	0. 5464	0. 5286	0. 5229
	0.001	0. 5296	0. 5337	0. 5369
	0.0001	0. 5384	0. 5396	0. 5402
Nadam	0.01	0. 5432	0. 5453	0. 5461
	0.001	0. 5466	0. 5461	0. 5460
Adagrad	0.0001	0. 5444	0. 5411	0. 5378
	0.01	0. 5378	0. 5373	0. 5366
	0.001	0. 5369	0. 5374	0. 5375
	0.0001	0. 5380	0. 5384	0. 5388

- [5] Kennedy, D.P., Courchesne, E.: The intrinsic functional organization of the brain is altered in autism. *Neuroimage* **39**(4), 1877–1885 (2008)
- [6] Wang, C., Xiao, Z., Wu, J.: Functional connectivity-based classification of autism and control using svm-rfecv on rs-fmri data. *Physica Medica* **65**, 99–105 (2019)
- [7] Khan, N.A., Waheeb, S.A., Riaz, A., Shang, X.: A three-stage teacher, student neural networks and sequential feed forward selection-based feature selection approach for the classification of autism spectrum disorder.

Table 41: Hyperparameter tuning for 250 neurons single layer GRU with Partial RSFC.

Optimizer	Learning rate	Batch size		
		4	8	16
Adam	0.01	0. 545	0. 5357	0. 535
	0.001	0. 5379	0. 5410	0. 5408
	0.0001	0. 5431	0. 5441	0. 5453
Nadam	0.01	0. 5474	0. 5491	0. 5511
	0.001	0. 5514	0. 5499	0. 5493
	0.0001	0. 5462	0. 5437	0. 5410
Adagrad	0.01	0. 5408	0. 5396	0. 5385
	0.001	0. 5391	0. 5398	0. 5401
	0.0001	0. 5406	0. 5410	0. 5413

Brain sciences **10**(10), 754 (2020)

- [8] Assaf, M., Jagannathan, K., Calhoun, V.D., Miller, L., Stevens, M.C., Sahl, R., O’Boyle, J.G., Schultz, R.T., Pearlson, G.D.: Abnormal functional connectivity of default mode sub-networks in autism spectrum disorder patients. *Neuroimage* **53**(1), 247–256 (2010)
- [9] Jones, T.B., Bandettini, P.A., Kenworthy, L., Case, L.K., Milleville, S.C., Martin, A., Birn, R.M.: Sources of group differences in functional connectivity: an investigation applied to autism spectrum disorder. *Neuroimage* **49**(1), 401–414 (2010)
- [10] Dadi, K., Rahim, M., Abraham, A., Chyzyk, D., Milham, M., Thirion, B., Varoquaux, G., Initiative, A.D.N., *et al.*: Benchmarking functional connectome-based predictive models for resting-state fmri. *NeuroImage* **192**, 115–134 (2019)
- [11] Parikh, M.N., Li, H., He, L.: Enhancing diagnosis of autism with optimized machine learning models and personal characteristic data. *Frontiers in Computational Neuroscience* **13**, 9 (2019). <https://doi.org/10.3389/fncom.2019.00009>
- [12] Dvornek, N.C., Ventola, P., Pelphrey, K.A., Duncan, J.S.: Identifying autism from resting-state fmri using long short-term memory networks. In: *International Workshop on Machine Learning in Medical Imaging*, pp. 362–370 (2017). Springer
- [13] Bilgen, I., Guvercin, G., Rezik, I.: Machine learning methods for brain network classification: application to autism diagnosis using cortical

- morphological networks. *Journal of neuroscience methods* **343**, 108799 (2020)
- [14] Kong, Y., Gao, J., Xu, Y., Pan, Y., Wang, J., Liu, J.: Classification of autism spectrum disorder by combining brain connectivity and deep neural network classifier. *Neurocomputing* **324**, 63–68 (2019)
- [15] Heinsfeld, A.S., Franco, A.R., Craddock, R.C., Buchweitz, A., Meneguzzi, F.: Identification of autism spectrum disorder using deep learning and the abide dataset. *NeuroImage: Clinical* **17**, 16–23 (2018)
- [16] Anirudh, R., Thiagarajan, J.J.: Bootstrapping graph convolutional neural networks for autism spectrum disorder classification. In: ICASSP 2019 - 2019 IEEE International Conference on Acoustics, Speech and Signal Processing (ICASSP), pp. 3197–3201 (2019). <https://doi.org/10.1109/ICASSP.2019.8683547>
- [17] Thomas, R.M., Gallo, S., Cerliani, L., Zhutovsky, P., El-Gazzar, A., van Wingen, G.: Classifying autism spectrum disorder using the temporal statistics of resting-state functional mri data with 3d convolutional neural networks. *Frontiers in psychiatry* **11**, 440 (2020)
- [18] El Gazzar, A., Cerliani, L., van Wingen, G., Thomas, R.M.: Simple 1-d convolutional networks for resting-state fmri based classification in autism. In: 2019 International Joint Conference on Neural Networks (IJCNN), pp. 1–6 (2019). IEEE
- [19] Sherkatghanad, Z., Akhondzadeh, M., Salari, S., Zomorodi-Moghadam, M., Abdar, M., Acharya, U.R., Khosrowabadi, R., Salari, V.: Automated detection of autism spectrum disorder using a convolutional neural network. *Frontiers in neuroscience* **13**, 1325 (2020)
- [20] Li, X., Dvornek, N.C., Papademetris, X., Zhuang, J., Staib, L.H., Ventola, P., Duncan, J.S.: 2-channel convolutional 3d deep neural network (2cc3d) for fmri analysis: Asd classification and feature learning. In: 2018 IEEE 15th International Symposium on Biomedical Imaging (ISBI 2018), pp. 1252–1255 (2018). IEEE
- [21] Tran, D., Bourdev, L., Fergus, R., Torresani, L., Paluri, M.: Learning spatiotemporal features with 3d convolutional networks. In: Proceedings of the IEEE International Conference on Computer Vision, pp. 4489–4497 (2015)
- [22] Subbaraju, V., Suresh, M.B., Sundaram, S., Narasimhan, S.: Identifying differences in brain activities and an accurate detection of autism spectrum disorder using resting state functional-magnetic resonance imaging: A spatial filtering approach. *Medical image analysis* **35**, 375–389 (2017)

- [23] Wang, Y., Wang, J., Wu, F.-X., Hayrat, R., Liu, J.: Aimafe: autism spectrum disorder identification with multi-atlas deep feature representation and ensemble learning. *Journal of Neuroscience Methods*, 108840 (2020)
- [24] Almuqhim, F., Saeed, F.: Asd-saenet: A sparse autoencoder, and deep-neural network model for detecting autism spectrum disorder (asd) using fmri data. *Frontiers in Computational Neuroscience* **15**, 27 (2021)
- [25] Dvornek, N.C., Ventola, P., Duncan, J.S.: Combining phenotypic and resting-state fmri data for autism classification with recurrent neural networks. In: 2018 IEEE 15th International Symposium on Biomedical Imaging (ISBI 2018), pp. 725–728 (2018). IEEE
- [26] Craddock, R.C., James, G.A., Holtzheimer III, P.E., Hu, X.P., Mayberg, H.S.: A whole brain fmri atlas generated via spatially constrained spectral clustering. *Human brain mapping* **33**(8), 1914–1928 (2012)
- [27] James, G., Witten, D., Hastie, T., Tibshirani, R.: *An Introduction to Statistical Learning* vol. 112. Springer, ??? (2013)
- [28] Friedman, J., Hastie, T., Tibshirani, R., *et al.*: *The Elements of Statistical Learning* vol. 1. Springer, ??? (2001)
- [29] Kuhn, M., Johnson, K., *et al.*: *Applied Predictive Modeling* vol. 26. Springer, ??? (2013)
- [30] Lipton, Z.C., Berkowitz, J., Elkan, C.: A critical review of recurrent neural networks for sequence learning. arXiv preprint arXiv:1506.00019 (2015)
- [31] Hochreiter, S.: The vanishing gradient problem during learning recurrent neural nets and problem solutions. *International Journal of Uncertainty, Fuzziness and Knowledge-Based Systems* **6**(02), 107–116 (1998)
- [32] Bengio, Y., Simard, P., Frasconi, P.: Learning long-term dependencies with gradient descent is difficult. *IEEE transactions on neural networks* **5**(2), 157–166 (1994)
- [33] Pascanu, R., Mikolov, T., Bengio, Y.: On the difficulty of training recurrent neural networks. In: *International Conference on Machine Learning*, pp. 1310–1318 (2013). PMLR
- [34] Hochreiter, S., Schmidhuber, J.: Long short-term memory. *Neural computation* **9**(8), 1735–1780 (1997)
- [35] Gers, F.A., Schmidhuber, J., Cummins, F.: Learning to forget: Continual prediction with lstm. 1999 Ninth International Conference on Artificial Neural Networks ICANN 99 (1999)

- [36] Gers, F.A., Schraudolph, N.N., Schmidhuber, J.: Learning precise timing with lstm recurrent networks. *J. Mach. Learn. Res.* **3**(null), 115–143 (2003). <https://doi.org/10.1162/153244303768966139>
- [37] Sherstinsky, A.: Fundamentals of recurrent neural network (rnn) and long short-term memory (lstm) network. *Physica D: Nonlinear Phenomena* **404**, 132306 (2020)
- [38] Bhandari, H.N., Rimal, B., Pokhrel, N.R., Rimal, R., Dahal, K.R., Khatri, R.K.: Predicting stock market index using lstm. *Machine Learning with Applications*, 100320 (2022)
- [39] Greff, K., Srivastava, R.K., Koutník, J., Steunebrink, B.R., Schmidhuber, J.: Lstm: A search space odyssey. *IEEE Transactions on Neural Networks and Learning Systems* **28**(10), 2222–2232 (2017). <https://doi.org/10.1109/TNNLS.2016.2582924>
- [40] Lei, J., Liu, C., Jiang, D.: Fault diagnosis of wind turbine based on long short-term memory networks. *Renewable Energy* **133**, 422–432 (2019). <https://doi.org/10.1016/j.renene.2018.10.031>
- [41] Lindemann, B., Müller, T., Vietz, H., Jazdi, N., Weyrich, M.: A survey on long short-term memory networks for time series prediction. *Procedia CIRP* **99**, 650–655 (2021)
- [42] Khullar, V., Salgotra, K., Singh, H.P., Sharma, D.P.: Deep learning-based binary classification of adhd using resting state mr images. *Augmented Human Research* **6**(1), 1–9 (2021)
- [43] Liu, R., Huang, Z.-a., Jiang, M., Tan, K.C.: Multi-lstm networks for accurate classification of attention deficit hyperactivity disorder from resting-state fmri data. In: 2020 2nd International Conference on Industrial Artificial Intelligence (IAI), pp. 1–6 (2020). IEEE
- [44] Dvornek, N.C., Li, X., Zhuang, J., Duncan, J.S.: Jointly discriminative and generative recurrent neural networks for learning from fmri. In: International Workshop on Machine Learning in Medical Imaging, pp. 382–390 (2019). Springer
- [45] El-Gazzar, A., Quaak, M., Cerliani, L., Bloem, P., van Wingen, G., Thomas, R.M.: A hybrid 3dcnn and 3dc-lstm based model for 4d spatio-temporal fmri data: an abide autism classification study. In: OR 2.0 Context-Aware Operating Theaters and Machine Learning in Clinical Neuroimaging, pp. 95–102. Springer, ??? (2019)
- [46] Cho, K., van Merriënboer, B., Çaglar Gülçehre, Bahdanau, D., Bougares, F., Schwenk, H., Bengio, Y.: Learning phrase representations using rnn

- encoder–decoder for statistical machine translation. In: EMNLP (2014)
- [47] Dey, R., Salem, F.M.: Gate-variants of gated recurrent unit (gru) neural networks. In: 2017 IEEE 60th International Midwest Symposium on Circuits and Systems (MWSCAS), pp. 1597–1600 (2017). IEEE
- [48] Chung, J., Gulcehre, C., Cho, K., Bengio, Y.: Empirical evaluation of gated recurrent neural networks on sequence modeling. arXiv preprint arXiv:1412.3555 (2014)
- [49] Pokhrel, N.R., Dahal, K.R., Rimal, R., Bhandari, H.N., Khatri, R.K., Rimal, B., Hahn, W.E.: Predicting nepse index price using deep learning models. *Machine Learning with Applications*, 100385 (2022)
- [50] Suthaharan, S.: Machine learning models and algorithms for big data classification. *Integr. Ser. Inf. Syst* **36**, 1–12 (2016)
- [51] Craddock, C., Benhajali, Y., Chu, C., Chouinard, F., Evans, A., Jakab, A., Khundrakpam, B.S., Lewis, J.D., Li, Q., Milham, M., et al.: The neuro bureau preprocessing initiative: open sharing of preprocessed neuroimaging data and derivatives. *Frontiers in Neuroinformatics* **7** (2013)
- [52] Bellec, P., Rosa-Neto, P., Lyttelton, O.C., Benali, H., Evans, A.C.: Multi-level bootstrap analysis of stable clusters in resting-state fmri. *Neuroimage* **51**(3), 1126–1139 (2010)
- [53] Pearson, K.: Correlation coefficient. In: Royal Society Proceedings, vol. 58, p. 214 (1895)
- [54] Beer, J.C., Aizenstein, H.J., Anderson, S.J., Krafty, R.T.: Incorporating prior information with fused sparse group lasso: Application to prediction of clinical measures from neuroimages. *Biometrics* **75**(4), 1299–1309 (2019) <https://arxiv.org/abs/https://onlinelibrary.wiley.com/doi/pdf/10.1111/biom.13075>. <https://doi.org/10.1111/biom.13075>
- [55] Kim, J., Wozniak, J.R., Mueller, B.A., Pan, W.: Testing group differences in brain functional connectivity: using correlations or partial correlations? *Brain connectivity* **5**(4), 214–231 (2015)
- [56] Artusi, R., Verderio, P., Marubini, E.: Bravais-pearson and spearman correlation coefficients: meaning, test of hypothesis and confidence interval. *The International journal of biological markers* **17**(2), 148–151 (2002)
- [57] Lever, J., Krzywinski, M., Altman, N.: Points of significance: Principal component analysis. *Nature methods* **14**(7), 641–643 (2017)
- [58] Altman, N., Krzywinski, M.: The curse (s) of dimensionality. *Nat Methods*

15(6), 399–400 (2018)

- [59] Pedregosa, F., Varoquaux, G., Gramfort, A., Michel, V., Thirion, B., Grisel, O., Blondel, M., Prettenhofer, P., Weiss, R., Dubourg, V., Vanderplas, J., Passos, A., Cournapeau, D., Brucher, M., Perrot, M., Duchesnay, E.: Scikit-learn: Machine learning in Python. *Journal of Machine Learning Research* **12**, 2825–2830 (2011)
- [60] Bhandari, H.N., Rimal, B., Pokhrel, N.R., Rimal, R., Dahal, K.R.: Lstm-sdm: An integrated framework of lstm implementation for sequential data modeling. *Software Impacts*, 100396 (2022)
- [61] Abadi, M., Agarwal, A., Barham, P., Brevdo, E., Chen, Z., Citro, C., Corrado, G.S., Davis, A., Dean, J., Devin, M., Ghemawat, S., Goodfellow, I., Harp, A., Irving, G., Isard, M., Jia, Y., Jozefowicz, R., Kaiser, L., Kudlur, M., Levenberg, J., Mané, D., Monga, R., Moore, S., Murray, D., Olah, C., Schuster, M., Shlens, J., Steiner, B., Sutskever, I., Talwar, K., Tucker, P., Vanhoucke, V., Vasudevan, V., Viégas, F., Vinyals, O., Warden, P., Wattenberg, M., Wicke, M., Yu, Y., Zheng, X.: TensorFlow: Large-Scale Machine Learning on Heterogeneous Systems. Software available from tensorflow.org (2015). <https://www.tensorflow.org/>